Adipose Mesenchymal Stem Cell-Derived Exosomes Promote the Regeneration of Corneal Endothelium Through Ameliorating Senescence

Yunkyoung Ryu,[1,2] Jin Sun Hwang,[1,2] Kyung Bo Noh,[1] Se Hie Park,[1,2] Je Hyun Seo,[3] and Young Joo Shin[1,2]

[1]Department of Ophthalmology, Hallym University Medical Center, Hallym University College of Medicine, Seoul, Republic of Korea
[2]Hallym BioEyeTech Research Center, Hallym University College of Medicine, Seoul, Republic of Korea
[3]Veterans Medical Research Institute, Veterans Health Service Medical Center, Seoul, Republic of Korea

Correspondence: Young Joo Shin, Department of Ophthalmology, Hallym University Medical Center, Hallym University College of Medicine, 1 Shingil-ro, Youngdeungpo-gu, Seoul 07441, Republic of Korea; schinn@hanmail.net.

YR and JSH are joint first authors.

Received: April 21, 2023
Accepted: September 14, 2023
Published: October 18, 2023

Citation: Ryu Y, Hwang JS, Bo Noh K, Park SH, Seo JH, Shin YJ. Adipose mesenchymal stem cell-derived exosomes promote the regeneration of corneal endothelium through ameliorating senescence. *Invest Ophthalmol Vis Sci.* 2023;64(13):29. https://doi.org/10.1167/iovs.64.13.29

Purpose. Human corneal endothelial cells (hCECs) have been considered unable to regenerate in vivo, resulting in corneal decompensation after significant loss of hCECs. adipose-derived mesenchymal stem cell (ASC)-derived exosomes can regenerate tissues and organs. In this study, we investigated whether ASC-derived exosomes could protect and regenerate CECs.

Methods. We performed cell viability and cell-cycle analyses to evaluate the effect of ASC-derived exosomes on the regeneration capacity of cultured hCECs. Transforming growth factor-β (TGF-β) and hydrogen peroxide (H_2O_2) were used to induce biological stress in CECs. The effect of ASC-derived exosomes on CECs was investigated in vivo. ASC-derived exosomes were introduced into rat CECs using electroporation, and rat corneas were injured using cryoinjury. Next-generation sequencing analysis was performed to compare the differentially expressed microRNAs (miRNAs) between ASC-derived and hCEC-derived exosomes.

Results. ASC-derived exosomes induced CEC proliferation and suppressed TGF-β- or H_2O_2-induced oxidative stress and senescence. ASC-derived exosomes protect hCECs against TGF-β- or H_2O_2-induced endothelial-mesenchymal transition and mitophagy. In an in vivo study, ASC-derived exosomes promoted wound healing of rat CECs and protected the corneal endothelium against cryoinjury-induced corneal endothelium damage. Next-generation sequencing analysis revealed differentially expressed miRNAs for ASC-derived and hCEC-derived exosomes. They are involved in lysine degradation, adherens junction, the TGF-β signaling pathway, the p53 signaling pathway, the Hippo signaling pathway, the forkhead box O (FoxO) signaling pathway, regulation of actin cytoskeleton, and RNA degradation based on Kyoto Encyclopedia of Genes and Genomes (KEGG) pathway analysis.

Conclusions. ASC-derived exosomes promoted wound healing and regeneration of endothelial cells by inducing a shift in the cell cycle and suppressing senescence and autophagy.

Keywords: corneal endothelial cells, adipose-derived mesenchymal stem cell, exosome

Human corneal endothelial cells (hCECs) do not regenerate in vivo, and their excessive loss results in corneal decompensation, which requires corneal transplantation.[1] Therefore, protecting and regenerating CECs should be the primary therapeutic goal for corneal endothelial diseases. However, such a treatment has not yet been developed.[2] The pathogenesis of CECs includes oxidative stress, endoplasmic reticulum (ER) stress, and RNA toxicity, which have been targeted for treatment.[3,4] One potential therapeutic strategy could be to inhibit senescence, because cell-cycle arrest in the G0/G1 phase, which is observed in CECs in vivo, resembles senescence.[5,6] Despite this, treatments that focus on CEC regeneration have not been developed.

Mesenchymal stem cells (MSCs) are stromal cells that are capable of self-renewal and multilineage differentiation.[7] The immunomodulatory and regenerative effects of MSCs are mediated by their paracrine activity.[8] Specially, MSCs secrete biologically active molecules, including cytokines and growth factors, such as interleukin (IL)-1, IL-10, tumor necrosis factor–stimulated gene-6 (TSG-6), fibroblast growth factor (FGF), hepatocyte growth factor (HGF), and platelet-derived growth factor (PDGF), which activate multiple signal transduction pathways. These pathways include phosphoinositide 3-kinase (PI3K)/Akt, Janus kinase (JAK)/signal transducer and activator of transcription (STAT), and mitogen-activated protein (MAP) kinase

pathways, which promote survival, proliferation, anti-apoptosis, and extracellular matrix remodeling.[8–10]

Exosomes are cell-derived vesicles present in many biological fluids that are reportedly involved in the paracrine effect of MSC and in cell–cell communication.[11] Adipose-derived mesenchymal stem cells (ASCs) secrete cytokines, growth factors, proteins, and extracellular vesicles and have great potential to regenerate tissues.[12,13] ASC-derived exosomes containing lipids, non-coding RNAs, microRNAs (miRNAs), DNA, heat shock proteins, and chaperones can alleviate ischemic injury and regenerate tissues and organs by modulating inflammation, senescence, ER stress, and oxidative stress.[14] They have potential therapeutic applications; however, the effect on CECs and the mechanism of action of ASC-derived exosomes remain unclear. Thus, in this study, we investigated the effect of ASC-derived exosomes on CEC regeneration. We found that TGF-β or oxidative stress induces senescence that inhibits the regeneration of CECs. Furthermore, we revealed that ASC-derived exosomes promote CEC regeneration by inhibiting TGF-β/oxidative stress–induced senescence. We also identified miRNAs derived from ASC-derived exosomes and analyzed their cellular mechanisms. Our findings provide a new therapeutic strategy for CEC.

Materials and Methods

Human CEC Culture

This study was performed in accordance with the tenets of the Declaration of Helsinki and was reviewed and approved by the institutional review board/ethics committee of the Hallym University Medical Center (NON2022-004). Cells were cultured according to previously published methods.[15–17] The corneas from three donors were used. A human CEC–Desçemet's membrane complex was incubated for 10 minutes in a solution of 0.25% trypsin/0.02% ethylenediaminetetraacetic acid (EDTA). The cells were then plated in six-well plates coated with a fibronectin–collagen (FNC) combination coating mix (Athena Environmental Sciences, Baltimore, MD, USA). Cells were cultured for 10 to 14 days until confluency and then passaged at a ratio of 1:3 using a 0.25% trypsin/0.02% EDTA solution.

Isolating and Labeling Exosomes From the Conditioned Medium

ASC-derived exosomes were prepared as previously described[18] and provided from Biosolution Co., Ltd. (Seoul, Korea).[18] For labeling with DiO, purified exosomes were incubated with DiO green fluorescence membrane dye (Invitrogen, Waltham, MA, USA) at a final concentration of 2 µg/mL for 1 hour at room temperature. The sample was further purified using the columns provided, and the exosomes were eluted in 200 µL of PBS. The exosomes were stored at −80°C until use. For microscopic analysis, cells grown on cover glasses were incubated with DiO-labeled exosomes in Gibco Opti-MEM (Thermo Fisher Scientific, Waltham, MA, USA) at 37°C for 6 hours. After incubation, the cells were washed with PBS to remove the unbound labeled exosomes and subsequently imaged using a fluorescence microscope (DMi8; Leica, Wetzlar, Germany).

Treating hCECs With ASC-Derived Exosomes

We seeded hCECs onto a 24-well culture plate at 4×10^4 cells per well and cultured them for 24 hours in growth medium at 37°C under 5% CO_2. The cells were then washed with PBS and treated with recombinant human TGF-β1 (10 ng/mL, ab50036; Abcam, Cambridge, UK) or H_2O_2 (1-mM) with or without ASC-derived exosomes (2×10^8 particles/mL, respectively) for 48 hours.

Cell Viability and Lactate Dehydrogenase Cytotoxicity Assay

Cells (1×10^4) were cultured in a 96-well plate and treated with ASC-derived exosomes for 48 to 72 hours. Cell viability was measured using a Cell Counting Kit-8 (CCK-8; Dojindo, Kumamoto, Japan) based on the water-soluble monosodium tetrazolium salt, WST-8 (2-[2-methoxy-4-nitrophenyl]-3-[4-nitrophenyl]-5-[2,4-disulfophenyl]-2H-tetrazolium). The plates were incubated with CCK-8 solution for 1 to 2 hours. Cell viability was determined by measuring absorbance at 450 nm using an Agilent BioTek Synergy HTX microplate reader (Agilent Technologies, Santa Clara, CA, USA) and expressed as the mean ± SD as a percentage of the control (100%). The experiments were repeated three times, and a representative experiment is shown (Fig. 2B).

The lactate dehydrogenase (LDH) cytotoxicity assay was performed using a commercial kit (MK401; Takara Bio, Otsu, Japan) according to the manufacturer's instructions. Cells (1×10^4 cells/well) were placed in 96-well plates and incubated for 48 hours in a humidified atmosphere containing 5% CO_2. The supernatant was transferred to new 96-well plates, mixed with reaction substrates, and incubated at 37°C for 30 minutes. Optical density was measured at 490 nm using the BioTek Synergy HTX microplate reader. Cytotoxicity was expressed as the fold change in the controls after subtracting the corresponding blanks.

Cell-Cycle Analysis

Cell-cycle analysis was performed using CytoFLEX flow cytometry (Beckman Coulter, Brea, CA, USA) with propidium iodide (PI) staining according to the manufacturer's protocol. The cells were harvested using trypsinization, washed with cold PBS, and fixed with cold 70% ethanol. The samples were stored at −20°C. Cells were treated with 50 µg/mL PI and 100 µg/mL RNase A.

Immunofluorescent Staining

hCECs were cultured on cover glasses in 12-well plates, washed with PBS, and fixed for 20 minutes in a 4% paraformaldehyde solution. The cells were permeabilized for 10 minutes with 0.5% Triton X-100 and blocked for 1 hour with 1% bovine serum albumin (BSA) at room temperature. After washing, the cells were incubated overnight with either mouse anti-mouse Ki67 (sc-23900; Santa Cruz Biotechnology, Santa Cruz, CA, USA) or goat anti-goat Nestin antibody (sc-21248; Santa Cruz Biotechnology) at 4°C and then washed with PBS. The cells were incubated with either fluorescein isothiocyanate–conjugated goat anti-rabbit IgG antibody or rabbit anti-goat antibody (1:100) for 1 hour at 37°C in the dark and then counterstained with Hoechst 33342 nuclear staining dye (1:2000; Molecular Probes, Eugene, OR, USA). After extensive washing with PBS, the slides

Investigative Ophthalmology & Visual Science

were mounted with a drop of mounting medium to reduce photobleaching. Negative control staining was conducted in parallel, omitting the primary antibodies. The slides were observed under the Leica DMi8 fluorescence microscope.

Quantitative Reverse-Transcription PCR

The miRNA was extracted using the mirPremier microRNA Isolation Kit (Sigma-Aldrich, St. Louis, MO, USA). First-strand cDNA was synthesized using a Mir-X miRNA First-Strand Synthesis Kit (Takara Bio). The real-time quantification of transcripts was performed on a LightCycler 96 (Roche Life Science, Mannheim, Germany) using the AccuPower 2X GreenStar qPCR Master Mix (Bioneer, Oakland, CA, USA). Quantitative reverse-transcription PCR (RT-qPCR) results were presented as fold changes relative to the control. The relative quantification was calculated using the ΔΔCT method. The relative expression was normalized to U6 small nuclear RNA (snRNA). The primers are described in Supplementary Table S1.

Mitochondrial Oxidative Stress Evaluation

Invitrogen MitoSOX Red was used to measure mitochondrial superoxide production.[19] The cells were incubated with 5-μM MitoSOX reagent for 10 minutes at 37°C in the dark. The fluorescence intensity in each well was measured using a CytoFLEX flow cytometer.

Senescence-Associated β-Galactosidase Assay

Senescence-associated β-galactosidase (SA-β-gal) staining was performed using a SA-β-gal staining kit (BioVision, Milpitas CA, USA).[20] Briefly, after the growth medium was removed from the cells, the cells were rinsed once with PBS. The fixative solution was added to each well, and the cells were fixed for 10 to 15 minutes at 25°C. After washing the cells with PBS, the cells were incubated in the β-galactosidase staining solution at 37°C overnight in a dry incubator.

Mitochondrial Membrane Potential Assay and Autophagosome Staining

JC-1 dye was used to obtain images of the mitochondrial membrane potential. We used the Muse MitoPotential assay (Merck Millipore, Burlington, MA, USA), which uses MitoPotential dye to detect changes in the mitochondrial membrane potential. The data were analyzed using a CytoFLEX flow cytometer. The cells were seeded in cover glass–bottom dishes, stained with the CYTO-ID Autophagy Detection Kit (Enzo Life Science, NY, USA) for 30 minutes, and then washed with PBS. The cells were observed under a Leica DMi8 fluorescence microscope.

Western Blot

Radioimmunoprecipitation assay buffer (Biosesang, Seoul, Korea) containing protease (Sigma-Aldrich) and phosphatase (PhosSTOP; Roche, Basel, Switzerland) inhibitor cocktails was used to isolate total cellular proteins. Western blotting was performed using standard protocols. We used 5% skim milk or gelatin to block non-specific binding for 1 hour. The primary antibodies were as follows: mouse anti-human N-cadherin antibody (1:500 dilution, sc-59987; Santa Cruz Biotechnology); mouse anti-human YAP antibody (1:500 dilution, sc-376830; Santa Cruz Biotechnology); rabbit anti-phospho-YAP antibody (1:500 dilution, PA5-17481; Invitrogen); mouse anti-LC3 antibody (1:1000 dilution, M186-3; MBL International Corporation, Woburn, MA, USA); or rabbit anti-GAPDH antibody (1:5000 dilution, LF-PA0212; Abfrontier, Seoul, Korea). Horseradish peroxidase (HRP)-conjugated secondary antibody and a WEST-Queen Western Blot Detection Kit (iNtRON Biotechnology, Seongnam, Korea) were used to detect the immunoreactive bands. Data were quantified using video image analysis (Luminograph II; Atto, Tokyo, Japan). Protein bands were measured using densitometry.

Animal Study

This study was approved by the Institutional Animal Care and Use Committee of Hallym University Medical Center (2021-3-0610-30). All procedures were performed according to the ARVO Statement for the Use of Animals in Ophthalmic and Vision Research. Six-week-old female Sprague Dawley rats (Raonbio, Yongin, Korea) were used for this procedure, and six Sprague Dawley rats were included in each group.

In Vivo Treatment of Rat CECs With Exosomes

ASC-derived exosomes (4.5×10^8/10 μL or 2.25×10^8/10 μL) or RNase-treated ASC-derived exosomes (4.5×10^8/10 μL) or hCEC-derived exosomes (4.5×10^8/10 μL) were injected into the anterior chamber of Sprague Dawley rats. A 7-mm-diameter tweezer electrode (BTX Harvard Apparatus, San Diego, CA, USA) was placed on both corneas, and electroporation was performed using the ECM 830 Square Wave Electroporation System (BTX, Cambridge, UK). The parameters for electroporation were as follows: five times, 100-ms duration each at 100 V with a 950-ms interval. Then, cryoinjury was employed to induce the corneal endothelial injury, which has been described previously,[21–23] in contact with a metal rod of 3-mm diameter for 15 seconds that had been frozen in liquid nitrogen for 10 minutes. Then, corneas were irrigated with normal saline.

Clinical Evaluation

Corneal opacity was evaluated using photographs obtained on days 2, 4, 7, 10, and 14. Corneal opacity was graded as follows: grade 0, no opacity; grade 1, mild opacity with visible iris detail; grade 2, moderate opacity with partial masking of the iris; and grade 3, severe opacity without a view of iris detail.

Alizarin Red S Staining

Vital staining was performed with 0.2% Alizarin Red S in 0.9% NaCl (pH 4.2) for 90 seconds, and the corneas were fixed in 2.5% glutaraldehyde. Corneal buttons were removed, placed on slides, and mounted under a coverslip with a drop of 0.9% NaCl. Corneal endothelium was observed under a Leica DMi8 light microscope. The cell density was then calculated.

Investigative Ophthalmology & Visual Science

miRNA Isolation and Sequencing

All procedures for next-generation sequencing (NGS) analysis were performed by Macrogen (Seoul, Korea). Exosomal miRNAs were extracted using the miRNeasy Serum/Plasma Kit (217184; QIAGEN, Hilden, Germany) after exosome extraction from the conditioned medium of hCECs using Exo2D-for RNA (EP-RU10; Exosomeplus, Seoul, Korea).

The samples were processed to produce exosomal RNA (10 ng) as an input for each library. Small RNA libraries were constructed using a SMARTer smRNA-Seq Kit for Illumina (Takara Bio), according to the manufacturer's guidelines. Sequencing libraries were constructed using polyadenylation, cDNA synthesis, and PCR amplification. cDNA fragments were sequenced by read length using a sequence-by-synthesis method on the Illumina platform.

Analysis of miRNA Expression Levels

After sequencing, raw sequence reads were filtered based on their quality. The adapter sequences were trimmed from the raw sequence reads. Ribosomal RNA (rRNA)-removed reads were sequentially aligned to the reference genome, miRBase 22.1, and non-coding RNA database, RNAcentral 14.0, to classify known miRNAs and other types of RNA such as transfer RNA (tRNA), snRNA, and small nucleolar RNA (snoRNA). Novel miRNA prediction was performed using miRDeep2. The raw data were normalized using the trimmed mean of the M-values (TMM) in edgeR. One was added to the normalized read count of the filtered miRNAs to facilitate log2 transformation and draw a correlation plot. For each miRNA, logCPM and log fold changes were calculated between the groups. We conducted a statistical hypothesis test to compare the two groups using the exactTest function in EdgeR. miRNAs differentially expressed between the two groups were defined as those with a fold change ≥ 2 and a raw P value of <0.05. We also performed hierarchical clustering analysis using complete linkage and Euclidean distance as measures of similarity to display the expression patterns of the differentially expressed miRNAs that satisfied the criteria of a fold change ≥ 2 and raw P value of <0.05. All data analysis and visualization of the differentially expressed genes were conducted using the R 3.6.2 program (R Foundation for Statistical Computing, Vienna, Austria).

Prediction of miRNA Targets and Functional Analysis of Differentially Expressed miRNAs

To investigate the biological role of the 12 dysregulated miRNAs, potential target genes were predicted using TargetScan 7.0 or microT-CDS 5.0 and DIANA Tools software.[24] Enrichment analysis, including pathway and functional annotation of differentially expressed miRNA target genes (MTGs) and dysregulated genes, was performed using the ShinyGo and DIANA-miRPath 3.0 web server.[24] To investigate the potential functional mechanism of the dysregulated miRNAs, we employed Kyoto Encyclopedia of Genes and Genomes (KEGG) pathway analysis[25,26] using the DIANA-miRPath 3.0 web server[24] with a false-discovery rate cutoff of $P = 0.05$.

Prediction Statistics

Data are expressed as mean ± SD. An independent t-test and one-way and two-way analyses of variance (ANOVAs) were used. All statistical analyses were performed using Prism 9.3.1 GraphPad, San Diego, CA, USA). Statistical significance was set at $P < 0.05$.

Results

Cellular Uptake of ASC-Derived Exosomes and Cell Proliferation

Initially, to investigate the uptake of exosomes, ASC-derived exosomes were stained with DiO for visualization and delivered using Opti-MEM I, a reduced serum medium. Transfected DiO-labeled exosomes were visualized with green fluorescence in hCECs using fluorescence microscopy (Fig. 1A). CCK-8 assays and cell-cycle analyses were performed to investigate whether ASC-derived exosomes affect cell viability or proliferation. Cell viability and cell-cycle analysis showed that ASC-derived exosomes induced the proliferation of hCECs and a shift in the cell cycle from the G0/G1 phase to the S phase in a dose-dependent manner (Figs. 1B–1F). RT-qPCR showed that miR-23a-3p and miR-302-3p were increased in exosome-treated cells (Fig. 1G).

ASC-Derived Exosomes Protect hCECs Against TGF-β- or H_2O_2-Induced Senescence

To investigate the effect of ASC-derived exosomes on cell viability under genotoxic stress, TGF-β or H_2O_2 was used to accelerate senescence,[27,28] and CCK-8 cell viability and LDH cytotoxicity were observed. TGF-β and H_2O_2 reduced cell viability and increased cytotoxicity that was alleviated by ASC-derived exosomes (Figs. 2A, 2B). We evaluated mitochondrial oxidative stress levels using the MitoSOX probe[29] and senescence using SA-β-gal staining (Figs. 2C–2F).[20] Mitochondrial oxidative stress levels and the number of SA-β-gal–positive cells increased after exposure to TGF-β or H_2O_2, demonstrating senescence and its associated reactions. ASC-derived exosomes alleviated the TGF-β- or H_2O_2-induced senescence in hCECs.

ASC-Derived Exosomes Protect hCECs Against TGF-β- or H_2O_2-Induced Endothelial–Mesenchymal Transition

We assessed the N-cadherin levels to investigate the effect of ASC-derived exosomes on endothelial–mesenchymal transition (EMT).[30] TGF-β or H_2O_2 upregulated N-cadherin levels, considered to be EMT markers, and ASC-derived exosomes alleviated this effect (Figs. 3A, 3B). We assessed the Hippo signaling pathway, which is responsible for the EMT and consists of pYAP and YAP.[31,32] pYAP was upregulated by ASC-derived exosomes (Figs. 3C, 3D), indicating activation of the Hippo signaling pathway. Furthermore, ASC-derived exosome–treated cells resulted in a decrease in the number of cells with YAP in the nucleus, although the exposure to TGF-β or H_2O_2 induced the nuclear translocation of YAP (Fig. 3F). To investigate whether inhibition of EMT by ASC-derived exosomes promoted proliferation, we performed immunofluorescence staining of Ki67, a prolifer-

Investigative Ophthalmology & Visual Science

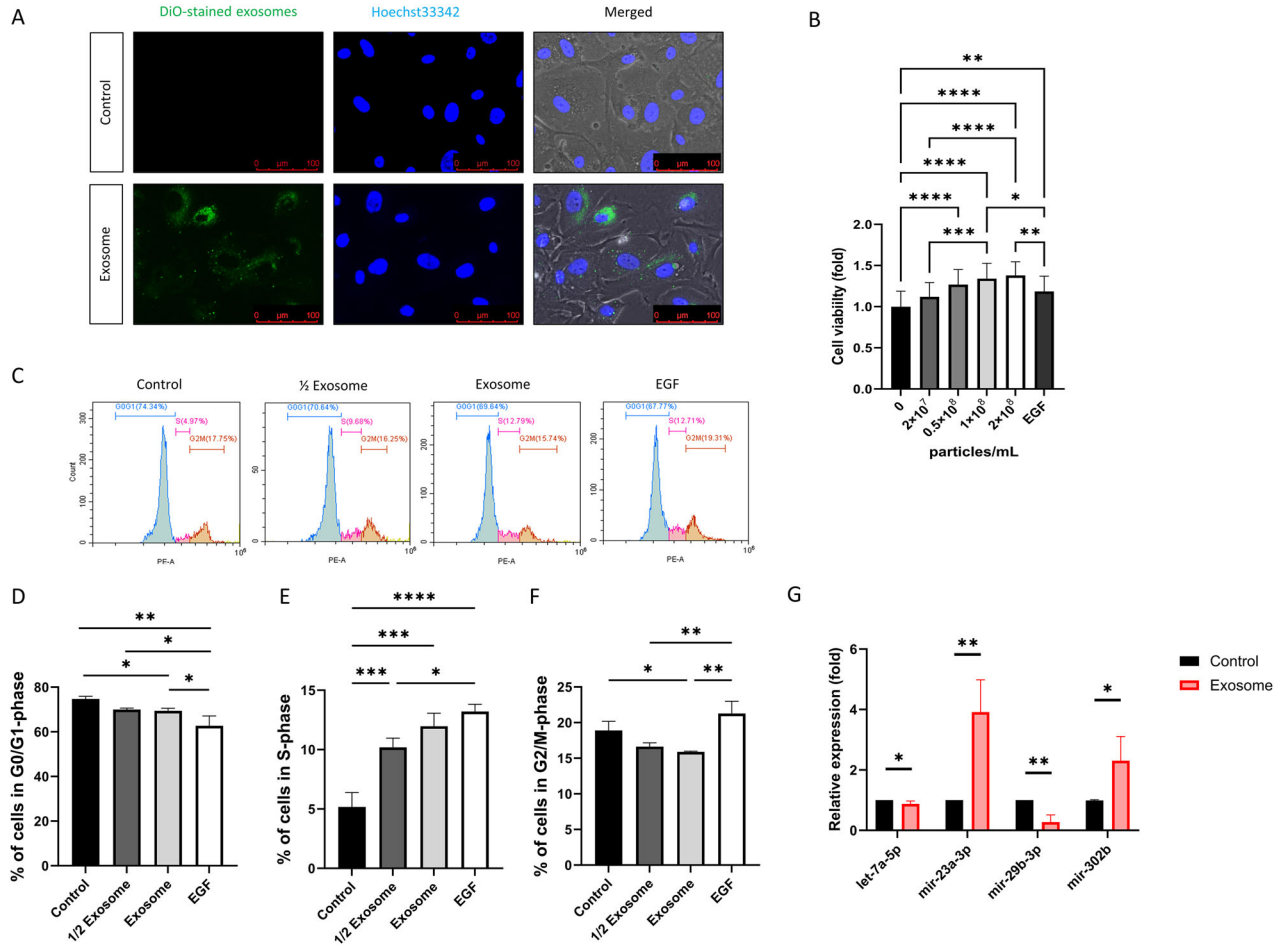

Figure 1. ASC-derived exosomes promote the proliferation of cultured CECs. (**A**) Uptake of DiO-labeled exosomes in cultured CECs is shown in *green*. *Scale bar:* 100 µm. (**B**) Cell viability was evaluated using the CCK-8 assay. (**C–F**) Cell cycles were analyzed using propidium iodide staining and flow cytometry. One-half exosome = 1×10^8 particles/mL. (**G**) RT-qPCR showed that miR-23a-3p and miR-302-3p were increased in exosome-treated cells. Data represent mean ± SD. *$P < 0.05$; **$P < 0.01$; ***$P < 0.001$.

ation marker. The ratio of Ki67-positive cells was increased by ASC-derived exosomes against TGF-β- or H_2O_2-induced EMT (Figs. 3G, 3H).

ASC-Derived Exosomes Protect hCECs Against TGF-β- or H_2O_2-Induced Mitophagy

To assess the effect of ASC-derived exosomes on cell death, we evaluated the mitochondrial membrane potential and autophagy. Mitochondrial membrane potential was visualized using JC-1 and assessed using the Muse MitoPotential Kit (EMD Millipore Corporation, Hayward, CA, USA) and flow cytometry (Figs. 4A–4C). TGF-β or H_2O_2 reduced the mitochondrial membrane potential, and this effect was alleviated by ASC-derived exosomes. Autophagy was investigated using an autophagy detection kit and western blotting of light chain 3 (LC3).[33] TGF-β and H_2O_2 significantly promote autophagosomes and the conversion of LC3I to LC3II that occurs during autophagy. ASC-derived exosomes attenuated TGF-β- or H_2O_2-induced autophagic responses.

Rat Corneal Endothelium Takes Up ASC-Derived Exosomes That Promote the Wound Healing In Vivo and Protect the Corneal Endothelium Against Cryoinjury-Induced Corneal Endothelium Damages

An animal experiment was performed to confirm the effects of ASC-derived exosomes. First, we determined whether ASC-derived exosomes could enter the rat corneal endothelium by electroporation. Exosomes stained with DiO—which stains the cell membrane—showed green fluorescence in the corneal endothelium of the exosome-injected group (Fig. 5A). Cryoinjury led to apoptosis, which was detected by TUNEL staining (Fig. 5B). After cryoinjury with liquid nitrogen, the corneas became opaque because of corneal endothelial damage. Corneal opacity decreased faster in the exosome-injected group (Figs. 5C, 5D). Corneal endothelial density, evaluated using Alizarin Red S staining, was increased in the exosome-injected group (Figs. 5E, 5F).

To confirm corneal endothelial regeneration, we performed immunofluorescence staining for Ki67, a proliferation marker.[34] Ki67-positive cells were more frequent in

Investigative Ophthalmology & Visual Science

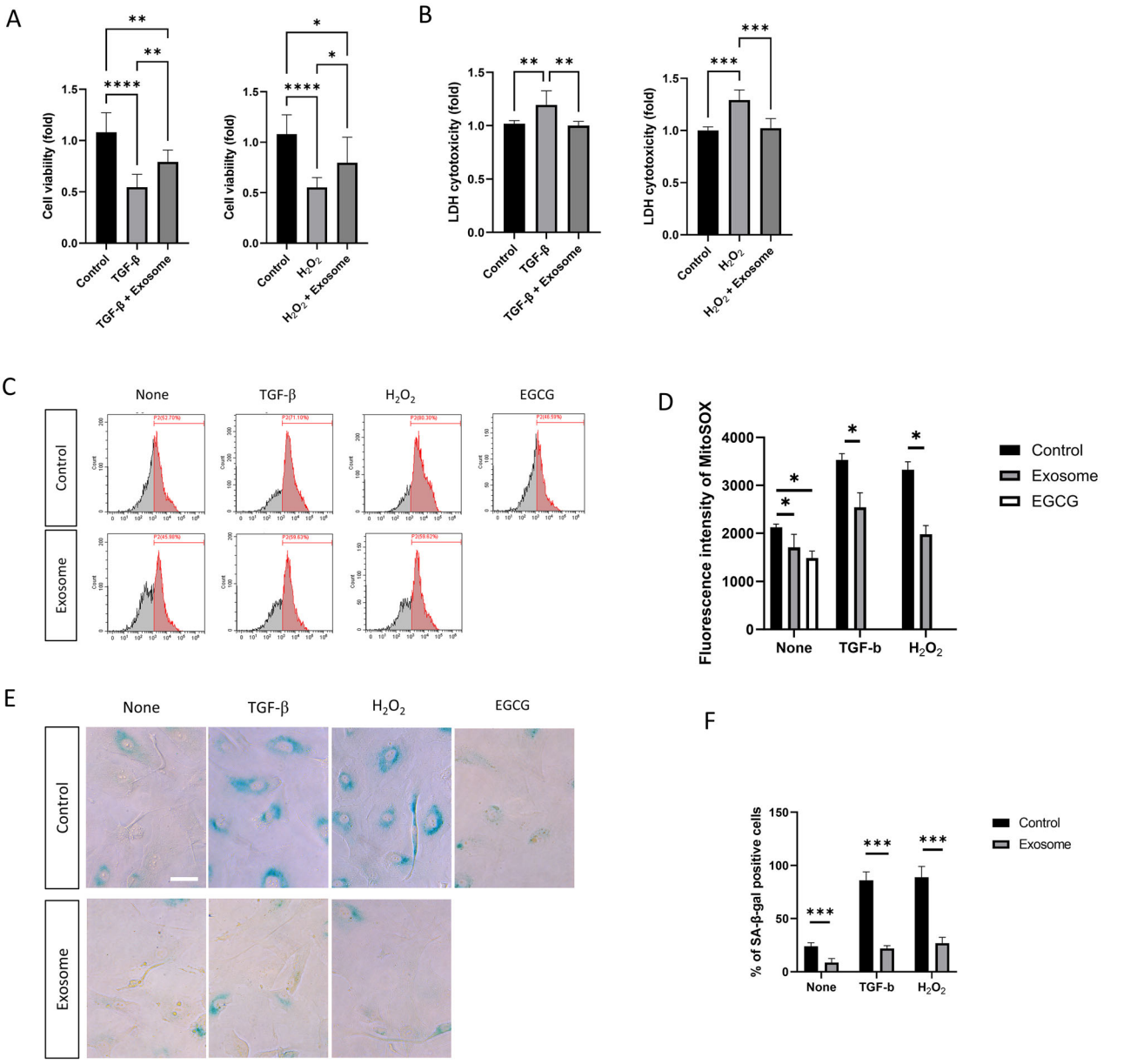

Figure 2. ASC-derived exosomes on TGF-β- or H_2O_2-induced senescence. (**A**) Cell viability was measured by CCK-8. (**B**) Cytotoxicity was assessed by lactate dehydrogenase (LDH) assay. (**C**, **D**) Mitochondrial oxidative stress level was measured using MitoSOX Red (500 nM of final concentration). The fluorescence intensity of MitoSOX was measured using a CytoFLEX flow cytometer. (**E**, **F**) Cellular senescence was assessed using senescence-associated β-galactosidase. *Blue* indicates SA-β-gal–positive senescent cells. *Scale bar:* 50 µm. Data represent mean ± SD. *$P < 0.05$; **$P < 0.01$; ***$P < 0.001$.

the exosome-injected group compared with the untreated group (Figs. 6A, 6B). To investigate stem cell activity, we performed immunofluorescence staining for Nestin, a neuroepithelial stem cell protein.[35] Nestin-positive cells were higher in numbers in the exosome-injected group compared with the untreated group (Figs. 6C, 6D). To investigate the mitochondrial membrane potential in vivo, JC-1 was used to stain mitochondria in the corneal endothelium of Sprague Dawley rats. The red fluorescence intensity, which indicates healthy and polarized mitochondria, was higher in the exosome group than in the control group (Fig. 6E). The MitoSOX red probe was used to assess mitochondrial oxidative stress levels in the corneal endothelium of Sprague Dawley rats. MitoSOX red intensity in the rat corneal endothelium was lower in the exosome group than in the control group, indicating lower oxidative stress in the former (Fig. 6F).

miRNAs in ASC-Derived Exosomes

We investigated the differences in miRNAs between ASC-derived- and hCEC-derived exosomes. The volcano plot (Fig. 7) shows the differences in miRNA expression levels between ASC-derived exosomes and hCEC-derived exosomes. The ASC-derived exosomes showed higher expression levels of hsa-miR-23a-5p, hsa-miR-196a-

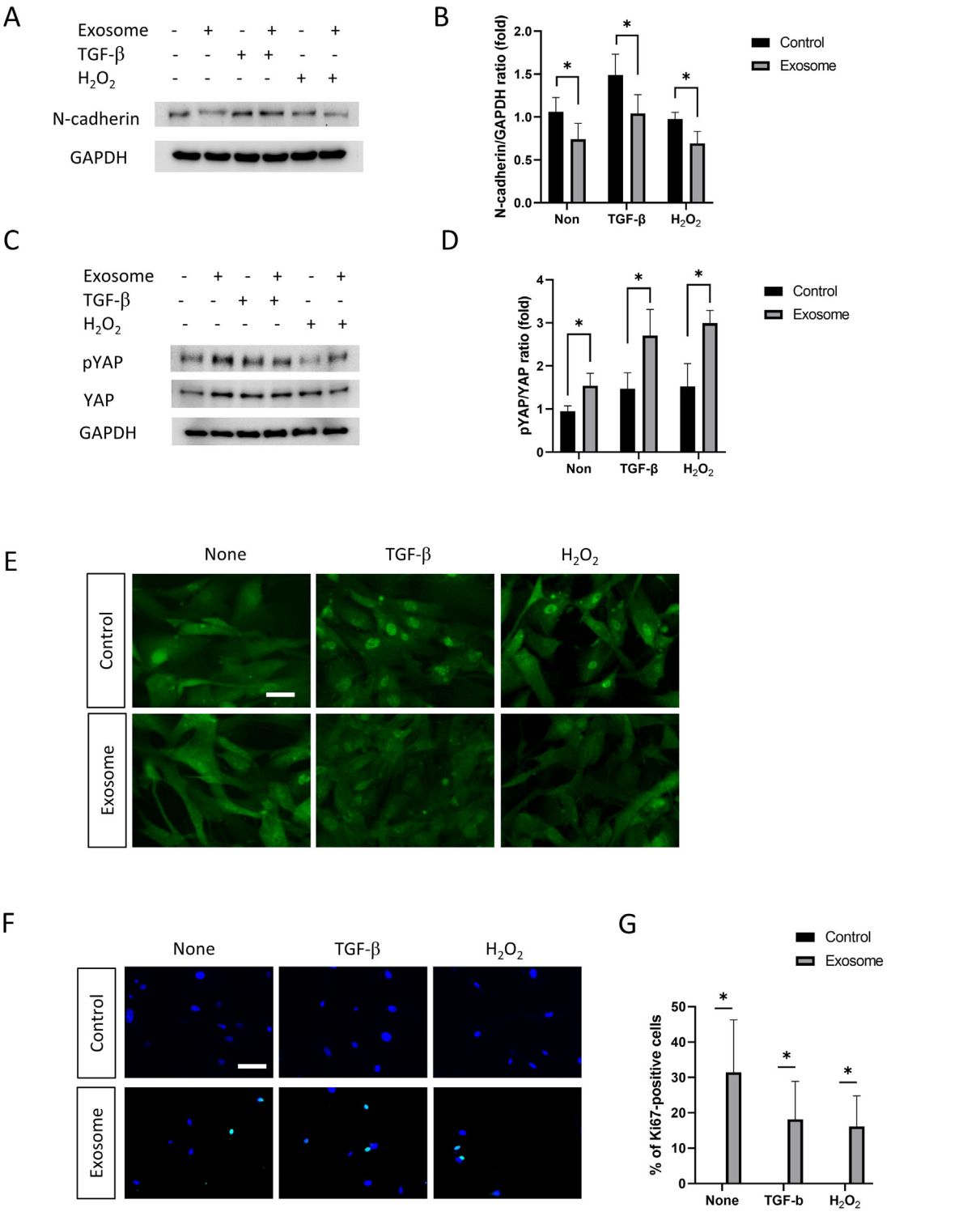

Figure 3. ASC-derived exosomes on TGF-β- or H_2O_2-induced endothelial-to-mesenchymal transition (EMT). (**A**, **B**) N-cadherin expression was evaluated by western blot analyses. (**C**, **D**) YAP and pYAP expression was evaluated by western blot analyses. (**E**) Immunofluorescence staining was used to evaluate the nuclear location of YAP. *Scale bar:* 50 µm. (**F**, **G**) Immunofluorescent staining of Ki67 was performed as a proliferation marker. *Scale bar:* 100 µm. Data represent mean ± SD. *$P < 0.05$.

5p, hsa-miR-4301, hsa-miR-489-3p, hsa-miR-1538, hsa-miR-6126, hsa-miR-762, hsa-miR-1246, hsa-miR-1228-5p, hsa-miR-193b-5p, hsa-miR-4647, hsa-miR-486-3p, hsa-miR-619-5p, hsa-miR-6511b-3p, hsa-miR-8485, hsa-miR-1306-5p, and hsa-miR-1290 (Table 1) and lower expression levels of hsa-miR-423-3p, hsa-miR-222-3p, hsa-miR-25-3p, hsa-miR-29b-3p, hsa-miR-143-3p, hsa-miR-21-5p, hsa-miR-23b-3p, hsa-miR-29a-3p, hsa-miR-221-3p, hsa-miR-186-5p, hsa-let-7f-5p, hsa-miR-130a-3p, hsa-miR-125a-5p, hsa-miR-34a-5p, hsa-miR-125b-5p, hsa-miR-7i-5p, hsa-miR-7e-5p, hsa-miR-199a-

Investigative Ophthalmology & Visual Science

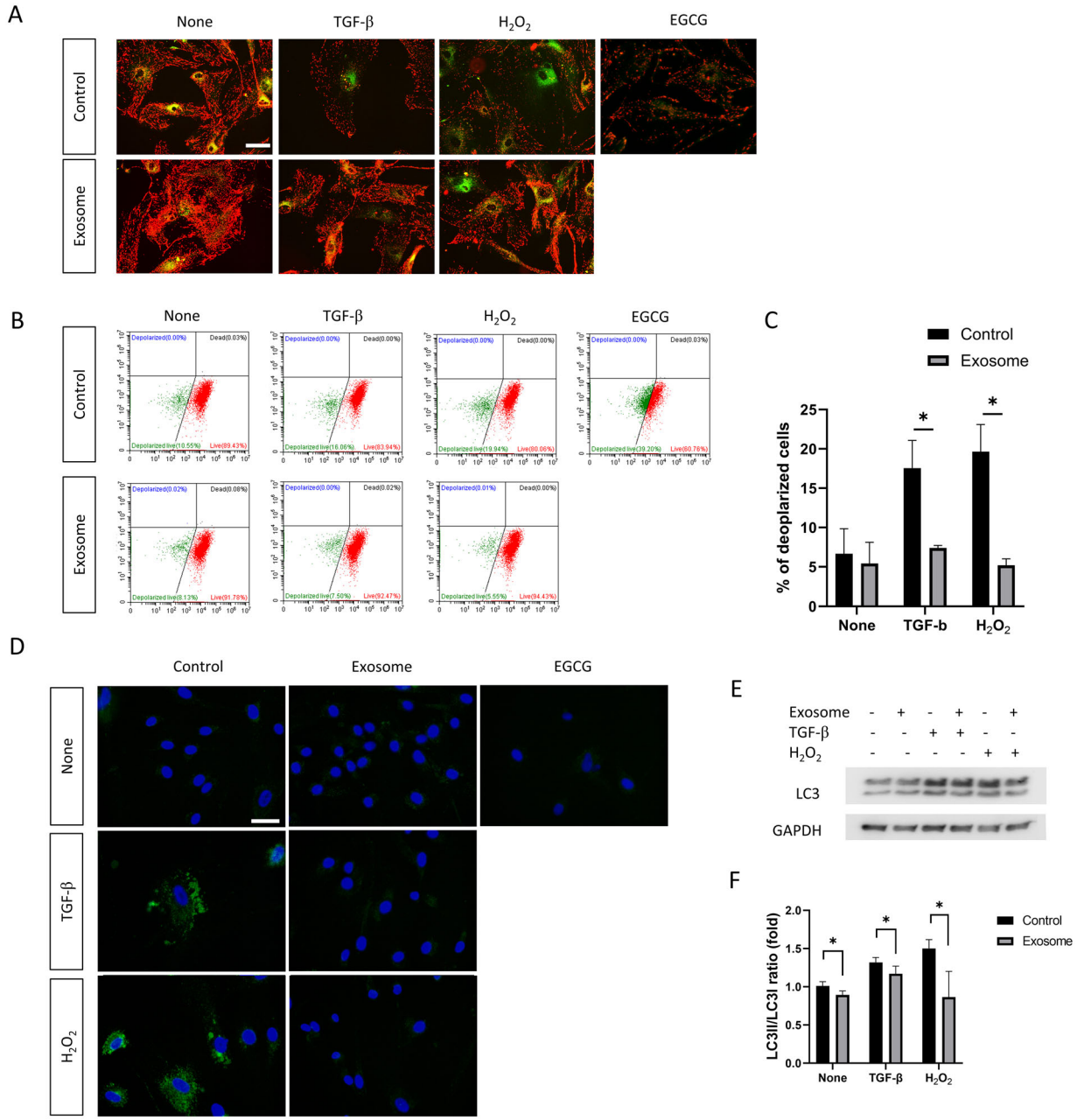

Figure 4. ASC-derived exosomes on TGF-β- or H_2O_2-induced mitophagy. (**A–C**) Mitochondrial membrane potential was imaged using a JC-1 probe (**A**) and measured using the Muse MitoPotential assay (**B**, **C**). *Scale bar:* 50 µm. (**D**) An autophagosome detection assay was used to assess autophagy. *Green* indicates autophagosome staining and *blue* indicates Hoechst 33342 nuclear staining. *Scale bar:* 50 µm. (**E**, **F**) Autophagy was assessed by the conversion of LC3I to LC3II using western blot analysis. Data represent mean ± SD. *$P < 0.05$; **$P < 0.01$; ***$P < 0.001$.

5p, hsa-miR-23a-3p, hsa-let-7a-5p, hsa-let-7a-3p, hsa-let-7g-5p, hsa-miR-191-5p, hsa-miR-199a-3p, hsa-miR-199b-3p, hsa-miR-574-3p, hsa-miR-24-3p, hsa-let-7d-5p, and hsa-miR-7b-5p than the hCEC-derived exosomes (Table 1).

We predicted the potential target genes of these differentially expressed miRNAs to further explore their function using miRbase and miRDB. The significant functions and signaling pathways in the KEGG pathway analysis were analyzed using miRPath 3.0. Pathway analysis of miRNAs overexpressed in ASC-derived exosomes showed lysine degradation, adherens junction, the TGF-β signaling pathway, the p53 signaling pathway, the Hippo signaling pathway, non-small cell lung cancer, the forkhead box O (FoxO) signaling pathway, regulation of actin cytoskeleton, and RNA degradation (Table 2). Pathway analysis of miRNAs underexpressed in ASC-derived exosomes showed lysine degradation, cell cycle, adherent junction, the Hippo signaling pathway, the p53 signaling pathway, the TGF-β signaling pathway, regulation of actin cytoskeleton, the Wnt signaling pathway, the FoxO signaling pathway, the mitogen-activated protein kinase (MAPK) signaling pathway, lysosomes, DNA replication, and apoptosis (Table 2).

Investigative Ophthalmology & Visual Science

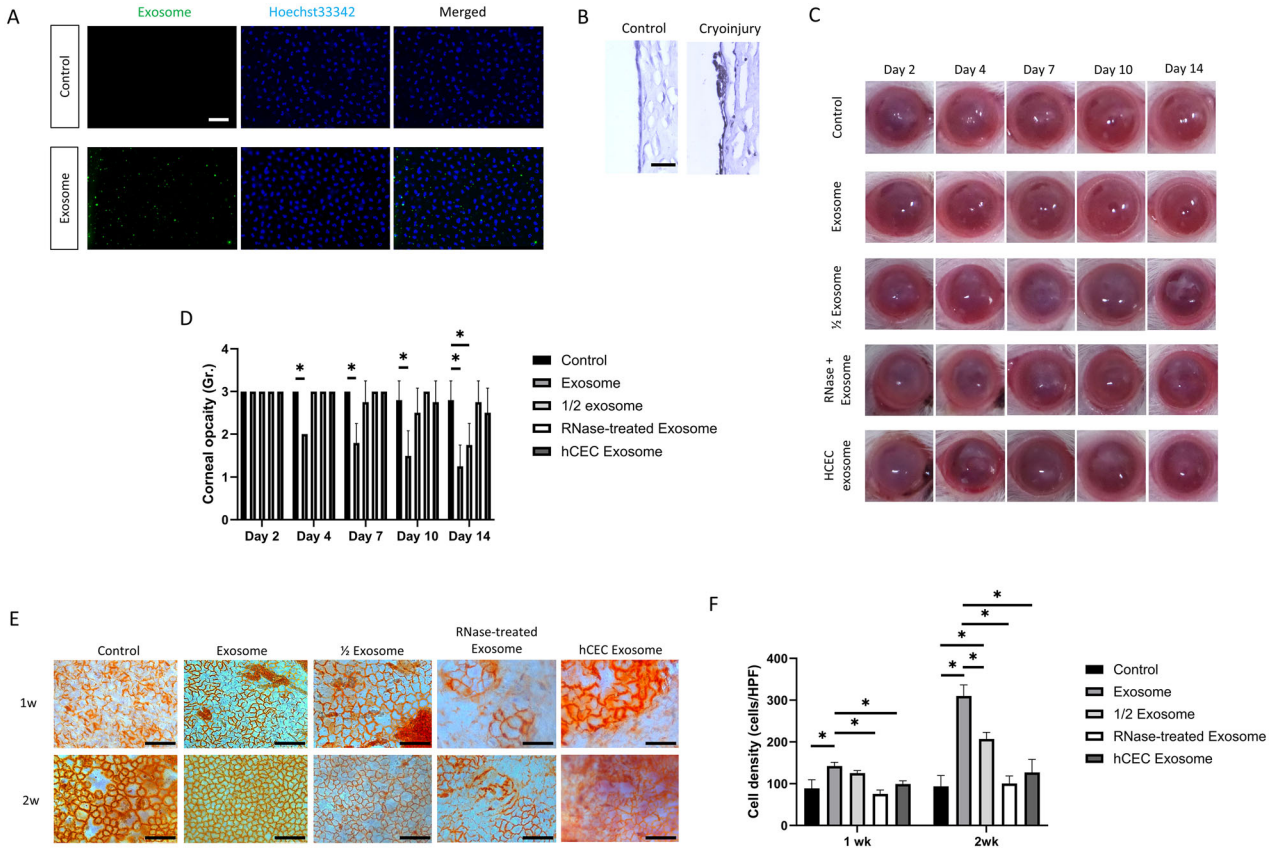

Figure 5. Protective effect of ASC-derived exosomes on cryoinjured corneal endothelium of rats. (**A**) Uptake of DiO-labeled exosome in rat corneal endothelium is shown in *green*. *Scale bar:* 50 µm. (**B**) TUNEL staining showed the apoptotic cells on the corneal endothelium after cryoinjury. (**C**, **D**) Corneal opacity was evaluated as time went on. (**E**, **F**) Corneal endothelial density was measured using Alizarin Red S staining. *Scale bar:* 100 µm. Data represent mean ± SD. $^{*}P < 0.05$; $^{**}P < 0.01$; $^{***}P < 0.001$.

Discussion

MSC-derived exosomes are known for their effectiveness in regenerating multiple organs.[36,37] Among MSCs, ASCs are readily available, safe, and effective for tissue regeneration and inflammation control.[38] ASC-derived exosomes have several advantages over ASCs, including smaller size, better tissue penetration, lack of cellular reactions, ease of storage, low immunogenicity, non-cytotoxicity, and non-mutagenic properties.[39] In this study, we investigated the effects and mechanisms of action of ASC-derived exosomes on promoting the wound healing and migration of CECs.

We first demonstrated that ASC-derived exosomes promoted wound healing and the migration of CECs both in vitro and in vivo. To create a CEC disease model through direct damage and secondary inflammatory responses, cryoinjury has been used to destroy CECs.[23,40,41] The activation of Nestin-stained stem cells by ASC-derived exosomes results in the promotion of wound healing of CECs, thereby improving the transparency of the rat cornea. ASC-derived exosomes have multiple biological activities due to their packed cell-type–specific combinations of proteins (cytoskeletal proteins, transmembrane proteins, and heat shock proteins), nucleic acids (DNA, mRNA, miRNA, and long and short non-coding RNA), lipids, and enzymes (GAPDH, ATPase, and pgk1), which shuttle these active cargoes between different cells that are involved in a complex intercellular communication system.[42,43] The miRNAs in ASC-derived exosomes, such as let-7a-5p, miR-23a-3p, miR-29b-3p, miR-302-3p, and miR-1246, regulate pluripotency, inhibit the EMT, and promote wound healing.[44] Using RT-qPCR, we showed that miR-23a-3p and miR-302-3p were increased in exosome-treated cells. TNF-stimulated gene 6 (TSG-6) and cytokines, such as IL-1 and IL-10, modulate the immune response, and growth factors, such as fibroblast growth factor (FGF), hepatocyte growth factor (HGF), and platelet-derived growth factor (PDGF), promote wound healing.[45–48] These factors are believed to have regenerative effects on the corneal endothelium.

In this study, we investigated the mechanism by which ASC-derived exosomes promoted the wound healing and migration of the corneal endothelium. We demonstrated that ASC-derived exosomes inhibit the EMT, which is a major mechanism that induces corneal endothelial dysfunction and opacity.[27,49] The EMT is induced by TGF-β and oxidative stress, which suppress tissue regeneration and promote corneal endothelial cell (CEC) dysfunction.[49,50] Hippo signaling, which is composed of yes-associated protein (YAP) and transcriptional coactivator with PDZ-binding motif (TAZ), is one of the signaling pathways of the EMT and induces the EMT in a transcriptional enhanced associate domain (TEAD)-dependent manner.[51] YAP in the nucleus increases the expression of EMT genes such as *SNAI*, *CTGF*, *BIRC5*, and *CYR61*.[51] YAP is degraded by ubiquitin-specific peptidase 9 X-linked (USP9X) after being phosphorylated to pYAP when

Investigative Ophthalmology & Visual Science

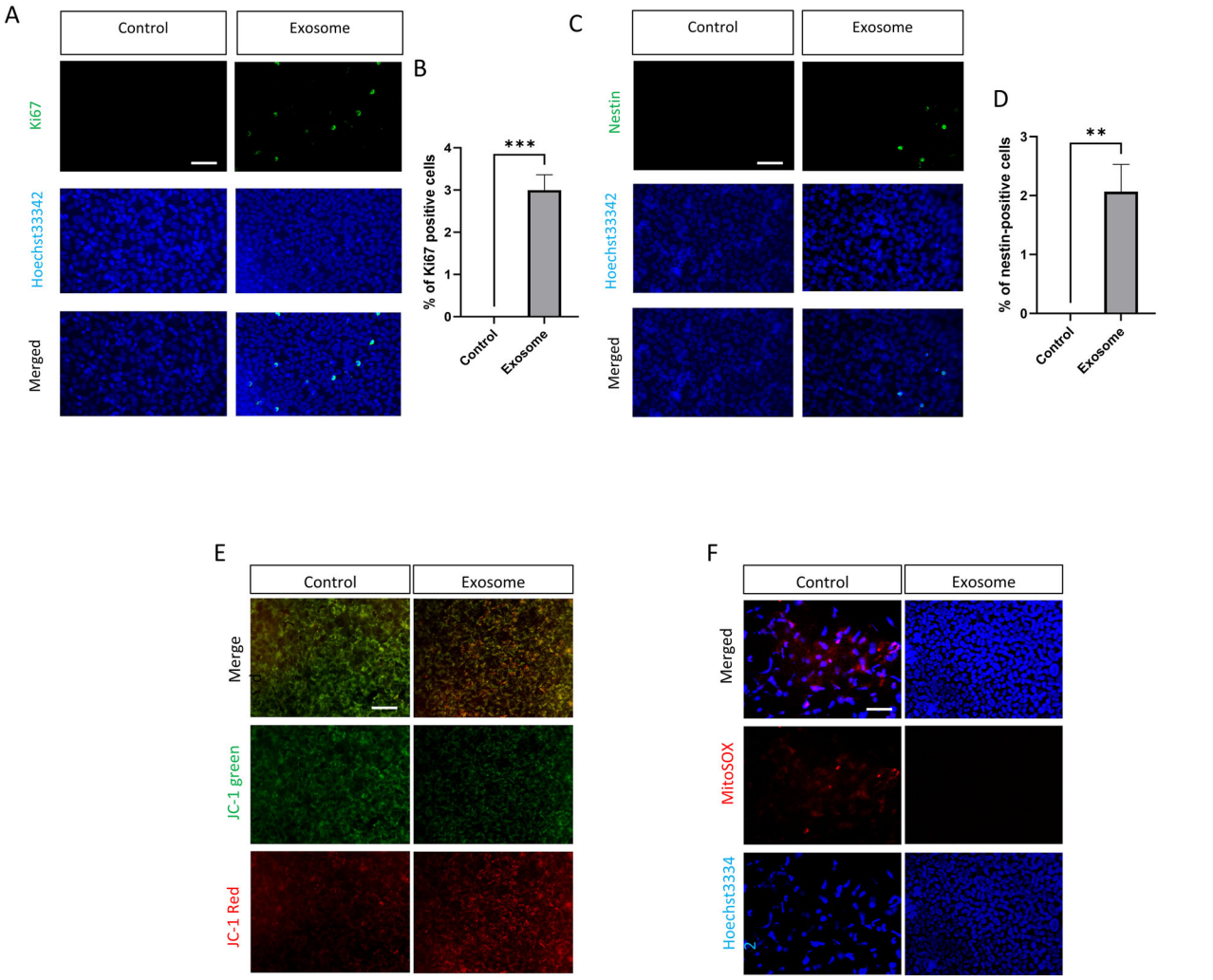

Figure 6. Regenerative effect of ASC-derived exosomes on cryoinjured corneal endothelium of rats. (**A**, **B**) Cells were stained with Ki67 as a proliferation marker. *Scale bar:* 50 µm. (**C**, **D**) Nestin expression was evaluated using immunofluorescence staining. *Scale bar:* 50 µm. (**E**) Mitochondrial membrane potential was assessed using JC-1 in rat corneal endothelium. *Scale bar:* 50 µm. One-half exosome = half dose of exosome group. (**F**) MitoSOX Red was used to evaluate the mitochondrial oxidation in rat corneal endothelium. *Scale bar:* 50 µm. Data represent mean ± SD. $^{*}P < 0.05$; $^{**}P < 0.01$; $^{***}P < 0.001$.

it emerges from the cytoplasm.[52] Thus, upregulation of pYAP results in suppression of the EMT.[31]

In addition to their inhibiting the EMT, we also showed that ASC-derived exosomes promote wound healing of the corneal endothelium by inhibiting senescence through the inhibition of reactive oxygen species (ROS). TGF-β and oxidative stress induce ROS, which in turn induces senescence and inhibits CEC regeneration by inducing cell hypertrophy and G0/G1 cell-cycle arrest.[27] ASC-derived exosomes downregulated senescence[53,54] and attenuated senescence-associated secretory phenotype-related activity through p16INK4a and IL-6.[54] Therefore, ASC-derived exosomes have the potential to regenerate the corneal endothelium by inhibiting the EMT and senescence.

Our study demonstrated that ASC-derived exosomes can improve senescence both in vitro and in vivo by improving mitochondrial function and inhibiting autophagy. Depolarization of the mitochondrial membrane potential indicates mitochondrial dysfunction, also observed in early cell death.[55] Mitochondria play a crucial role in the survival and function of CECs, which require a significant amount of energy to maintain dehydration of the corneal stroma.[55] Oxidative stress and mitochondrial dysfunction are known to promote senescence, and we observed that ASC-derived exosomes improved mitochondrial integrity and reduced ROS levels in CECs. Specifically, ASC-derived exosomes restored mitochondrial function by transporting mitochondrial proteins, lipids, and mtDNA to and from the organelle.

Autophagy is a type of cell death that can contribute to cell survival through recycling biomolecules. However, autophagy can also inhibit cell proliferation and regeneration.[56] In this study, we found that ASC-derived exosomes inhibited autophagy, which contributed to CEC regeneration. The EMT is associated with mitochondrial dysfunction, increased ROS levels, and decreased mitochondrial membrane potential.[57,58] Autophagy promotes the EMT through TGF-β–dependent signaling.[59,60] Therefore, inhibiting autophagy inhibits the EMT and restores mitochondrial function, leading to CEC regeneration.

Investigative Ophthalmology & Visual Science

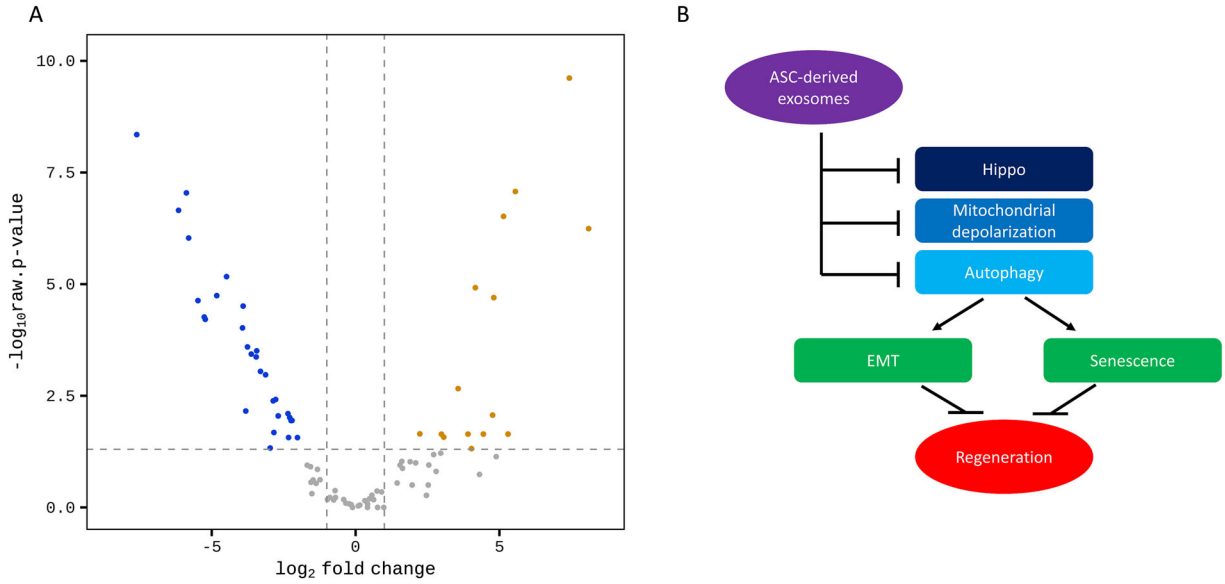

Figure 7. (**A**) Differentially expressed miRNA between ASC-derived exosomes and hCEC-derived exosomes. Volcano plot shows ASC-derived exosomes versus hCEC-derived exosomes. (**B**) Schematic diagram.

Cryoinjury has been used to cause injury in CECs in the in vivo model, which stimulates the Stk11-p53 signaling pathway as well as apoptosis.[21,40] In this study, apoptosis was elevated in response to cryoinjury-induced cellular damage and CEC density was reduced in cryoinjured cornea. Cryoinjury induces desquamation of CECs into the anterior chamber, and apoptosis helps to clear the damaged cells.[23,61]

Previously, the effects of MSC-derived extracellular vesicles (EV) and blood serum–derived EVs were compared.[62] The study showed that EVs inhibited tunicamycin-induced ER stress and apoptosis, improving the survival of CECs.[62,63] Different from that study, our study revealed that ASC EVs promote the proliferation of CECs and suppress TGF-β- and H_2O_2-induced senescence through regulation of Hippo signaling, mitochondrial function, and autophagy. A schematic diagram is shown in Figure 7B.

In this study, we investigated the differentially expressed miRNAs between ASC-derived and hCEC-derived exosomes and summarized the related pathways in Table 2. The differentially expressed miRNAs are associated with lysine degradation, proliferation, the TGF-β signaling pathway, the p53 signaling pathway, the Hippo signaling pathway, the FoxO signaling pathway, and regulation of the actin cytoskeleton. Lysine degradation occurs in the mitochondria and regulates mitochondrial energy production.[64,65] In this study, we showed that ASC-derived exosomes activate mitochondrial function. Furthermore, ASC-derived exosomes were shown to inhibit the TGF-β and Hippo signaling pathways, as well as senescence, which is associated with the p53 signaling pathway.

The functions of several miRNAs overexpressed in ASC-derived exosomes have been previously described. miR-8485 activates the Wnt/β-catenin pathway[66] and promotes cell proliferation and migration.[67] miR-1298 attenuates myocardial ischemia–reperfusion injury by targeting protein phosphatase 2,[68] protecting cells against damage caused by chronic oxidative stress by inhibiting the TGF-β_2/Smad4 pathway, activating the canonical Wnt pathway, and inhibiting autophagy.[69] miR-619-5p promotes proliferation and suppresses the PTEN/AKT/p21 pathway.[70] miR-486-3p is regulated by the TGF-β/SMAD pathway and exerts an antifibrotic effect.[71] miR-193b is downregulated by TGF-β1 and regulates TGF-β signaling by targeting the TGF-β receptor type 3.[71–73] miR-1228 prevents cellular apoptosis[74] and suppresses the EMT.[75] miR-762 is predominantly translocated to the mitochondria and participates in regulation of mitochondrial function.[76] miR-489-3p regulates the oxidative stress response,[77] inhibits Toll-like receptor 4/NF-κB signaling to prevent inflammation,[78] and reduces the expression of profibrotic markers induced by TGF-β1.[79] miR-196a-5p modulates gastric cancer stem cell–like characteristics by targeting SMAD4 and mitigating renal fibrosis by targeting TGF-β receptor 2.[80,81] miRNA-23a regulates the EMT in endometrial endometrioid adenocarcinoma by targeting SMAD3.[82] miR-1306-5p targets TGF-β receptor 2 and inhibits the transcription factor SMAD4.[83] miR-1290 regulates stemness by targeting the retinoic acid receptor-related orphan receptor A (RORA).[84]

Furthermore, miRNAs downregulated in ASC-derived exosomes compared with hCEC-derived exosomes have been described. Most of them, including hsa-let-7d-5p, hsa-let-7e-5p, hsa-let-7f-5p, hsa-let-7i-5p, hsa-let-7a-5p, hsa-miR-23a-3p, hsa-miR-34a-5p, hsa-miR-122-5p, hsa-miR-125a-3p, hsa-miR-125a-5p, hsa-miR-125b-5p, hsa-miR-181a-5p, hsa-miR-221-3p, hsa-miR-222-3p, hsa-miR-574-3p, and hsa-miR-574-5p, have been reported to be upregulated in senescent cells.[85–87] miR-423-3p drives the EMT by targeting CYBRD1.[88] miR-222-3p promotes the EMT by targeting E-cadherin and Notch signaling.[89,90] miR-25-3p regulates oxidative stress by upregulating NOX4.[91] miR-29 induces cellular senescence through multiple signaling pathways[92] and promotes particulate matter–induced inflammatory responses by regulating the AMP-activated protein kinase (AMPK) pathway.[93] miR-143-3p is a TGF-β-inducible miRNA [94,95] that indirectly and negatively regulates ER stress.[96] miR-130a-3p inhibits the TGF-β–induced EMT via SMAD4.[97,98] miR-21 is involved in the TGF-β1 signaling pathway[99] and suppresses the Hippo signaling pathway.[100] miR-23b-3p acti-

Table 1. Identification of Differentially Expressed miRNAs in ASC-Derived Exosomes Via RNA Sequencing

miRNA	False-Discovery Rate	Log_2 Fold Change	Regulation
hsa-let-7i-5p	2.1727E-07	−194.897901	Down
hsa-miR-221-3p	4.3158E-06	−71.184344	Down
hsa-miR-29a-3p	2.1916E-06	−58.921689	Down
hsa-miR-24-3p	1.1229E-05	−55.782975	Down
hsa-miR-130a-3p	0.00017438	−44.609079	Down
hsa-miR-149-5p	0.00035217	−38.343655	Down
hsa-miR-186-5p	0.00037198	−37.367225	Down
hsa-let-7d-5p	0.00015943	−28.352306	Down
hsa-let-7f-5p	7.3161E-05	−22.390628	Down
hsa-let-7g-5p	0.00054502	−15.245191	Down
hsa-let-7a-5p	0.00021477	−15.017823	Down
hsa-miR-423-3p	0.02493622	−14.095648	Down
hsa-miR-222-3p	0.00137105	−13.518604	Down
hsa-miR-21-5p	0.00178572	−12.336949	Down
hsa-miR-191-5p	0.00196918	−10.959173	Down
hsa-miR-23b-3p	0.00159189	−10.825331	Down
hsa-miR-25-3p	0.00396424	−9.888494	Down
hsa-let-7e-5p	0.00451741	−8.744121	Down
hsa-miR-143-3p	0.098648082	−7.830223	Down
hsa-miR-29b-3p	0.01532825	−7.280391	Down
hsa-let-7a-3p	0.052913094	−7.155717	Down
hsa-miR-199a-5p	0.01486005	−6.852863	Down
hsa-miR-199a-3p	0.02793724	−6.450906	Down
hsa-miR-199b-3p	0.02793724	−6.450906	Down
hsa-miR-23a-3p	0.02751576	−5.096368	Down
hsa-miR-34a-5p	0.058889291	−5.026538	Down
hsa-miR-125b-5p	0.02940564	−4.888319	Down
hsa-miR-574-3p	0.03235707	−4.732195	Down
hsa-let-7b-5p	0.03235707	−4.622342	Down
hsa-miR-125a-5p	0.058889291	−4.056346	Down
hsa-miR-193b-5p	0.052913094	4.700097	Up
hsa-miR-1306-5p	0.052913094	7.906345	Up
hsa-miR-23a-5p	0.058889291	8.370368	Up
hsa-miR-619-5p	0.00883593	11.831495	Up
hsa-miR-762	0.052913094	15.001013	Up
hsa-miR-6511b-3p	0.099515986	16.319879	Up
hsa-miR-6126	0.00011642	17.918932	Up
hsa-miR-1538	0.052913094	21.725345	Up
hsa-miR-409-3p	0.052913094	21.725345	Up
hsa-miR-486-3p	0.02793724	27.130810	Up
hsa-miR-4301	0.00016199	27.937320	Up
hsa-miR-1246	4.913E-06	35.320756	Up
hsa-miR-1228-5p	0.052913094	39.375945	Up
hsa-miR-4647	0.052913094	39.375945	Up
hsa-miR-1290	2.1916E-06	46.983113	Up
hsa-miR-8485	2.3535E-08	172.464431	Up
hsa-miR-196a-5p	7.9199E-06	274.506271	Up

vates TGF-β signaling by increasing SMAD2 phosphorylation[101] and regulates autophagy by suppressing SIRT1.[102] miR-29, miR-143, and miR-21 inhibit mitophagy.[3,103,104] miR-221-3p facilitates the EMT and promotes cell migration.[105] miR-186-5p inhibits cell proliferation and induces apoptosis.[106] miR-138a-3p induces senescence in renal carcinoma cells by targeting enhancer of zeste homolog 2 (EZH2)[107] and reinforces two separate senescence-regulating branches in progerin-expressing endothelial cells: the p53- and p16-associated pathways.[108] miR-199a-3p/5p participates in TGF-β- and epidermal growth factor (EGF)-induced EMT by targeting DUSP5/MAP3K11.[109] miR-191-5p is induced by hypoxia and regulates TGF-β signaling.[110,111] miR-199b-3p suppresses the growth and progression of ovarian cancer via the EMT signaling pathway by targeting ZEB1.[112] miR-574-3p is induced by TGF-β1 and induces apoptosis.[72,113] miR-24-3p inactivates the Hippo signaling pathway.[114]

A gene ontology is shown in Table 3. TGF-β and HIPPO signaling were investigated in this study to assess the function of selected miRNAs in exosomes. The functions of individual miRNAs will be elucidated in future studies.

In conclusion, our findings demonstrate that ASC-derived exosomes have the potential to improve the wound healing and migration of CECs by inducing a shift in the cell cycle and inhibiting senescence and autophagy pathways. Hence, these exosomes may serve as a promising therapeutic approach for the treatment of CEC diseases.

Investigative Ophthalmology & Visual Science

Table 2. Enriched KEGG Pathways Regulated by miRNAs Overexpressed or Underexpressed in ASC-Derived Exosomes

Pathway	miRNAs	*P*
Overexpressed miRNA		
Lysine degradation	hsa-miR-486-3p, hsa-miR-196a-5p, hsa-miR-1246, hsa-miR-193b-5p, hsa-miR-1290, hsa-miR-1306-5p	3.11e-09
Adherens junction	hsa-miR-196a-5p, hsa-miR-193b-5p, hsa-miR-486-3p, hsa-miR-1290, hsa-miR-1306-5p, hsa-miR-23a-5p	1.19e-05
TGF-β signaling pathway	hsa-miR-196a-5p, hsa-miR-23a-5p, hsa-miR-193b-5p, hsa-miR-1246, hsa-miR-1290, hsa-miR-1306-5p	0.0020
p53 signaling pathway	hsa-miR-196a-5p, hsa-miR-193b-5p, hsa-miR-486-3p, hsa-miR-1246, hsa-miR-1290, miR-1306-5p	0.0151
Hippo signaling pathway	hsa-miR-196a-5p, hsa-miR-193b-5p, hsa-miR-1246, hsa-miR-486-3p, hsa-miR-23a-5p, hsa-miR-1306-5p, hsa-miR-1290	0.0012
FoxO signaling pathway	hsa-miR-196a-5p, hsa-miR-1246, hsa-miR-23a-5p, hsa-miR-486-3p, hsa-miR-193b-5p, hsa-miR-1306-5p, hsa-miR-1290	0.0015
Regulation of actin cytoskeleton	hsa-miR-196a-5p, hsa-miR-1246, hsa-miR-1228-5p, hsa-miR-486-3p, hsa-miR-193b-5p, hsa-miR-1306-5p, hsa-miR-1290	0.0158
Signaling pathways regulating pluripotency of stem cells	hsa-miR-196a-5p, hsa-miR-193b-5p, hsa-miR-1246, hsa-miR-1228-5p, hsa-miR-23a-5p, hsa-miR-1306-5p, hsa-miR-1290	0.0264
Underexpressed miRNA		
Lysine degradation	hsa-miR-34a-5p, hsa-miR-21-5p, hsa-miR-23b-3p, hsa-miR-23a-3p, hsa-miR-423-3p, hsa-miR-222-3p, hsa-miR-25-3p, hsa-miR-221-3p, hsa-miR-186-5p, hsa-miR-130a-3p, hsa-miR-125a-5p, hsa-miR-125b-5p, hsa-miR-24-3p, hsa-let-7a-5p, hsa-let-7i-5p, hsa-let-7e-5p, hsa-miR-29b-3p, hsa-miR-29a-3p, hsa-let-7f-5p, hsa-let-7g-5p, hsa-miR-143-3p, hsa-miR-191-5p, hsa-miR-199a-3p, hsa-miR-199b-3p, hsa-let-7d-5p, hsa-let-7b-5p, hsa-miR-199a-5p	8.14E-8
Cell cycle	hsa-miR-25-3p, hsa-let-7f-5p hsa-let-7i-5p, hsa-let-7e-5p, hsa-let-7a-5p, hsa-let-7g-5p, hsa-miR-186-5p, hsa-miR-23b-3p hsa-miR-125a-5p, hsa-miR-125b-5p, hsa-miR-23a-3p, hsa-miR-222-3p, hsa-miR-221-3p, hsa-miR-34a-5p, hsa-miR-130a-3p, hsa-miR-423-3p, hsa-miR-143-3p, hsa-miR-29b-3p, hsa-miR-29a-3p, hsa-miR-199a-3p, hsa-let-7b-5p, hsa-miR-21-5p, hsa-miR-24-3p, hsa-miR-199a-5p, hsa-let-7d-5p, hsa-let-7a-3p, hsa-miR-191-5p, hsa-miR-199b-3p	7.17E-10
Adherens junction	hsa-let-7f-5p, hsa-let-7i-5p, hsa-let-7a-5p, hsa-let-7g-5p, hsa-miR-23b-3p, hsa-miR-25-3p, hsa-miR-221-3p, hsa-let-7e-5p, hsa-miR-24-3p hsa-miR-130a-3p, hsa-miR-21-5p, hsa-miR-29a-3p, hsa-miR-186-5p, hsa-miR-34a-5p, hsa-miR-23a-3p, hsa-miR-143-3p, hsa-miR-199a-3p, hsa-miR-125a-5p, hsa-miR-125b-5p, hsa-miR-199a-5p, hsa-let-7b-5p, hsa-miR-191-5p, hsa-miR-199b-3p, hsa-miR-222-3p, hsa-miR-29b-3p, hsa-let-7d-5p, hsa-let-7a-3p, hsa-miR-423-3p	1.33E-09
Hippo signaling pathway	hsa-let-7e-5p, hsa-let-7a-5p, hsa-miR-34a-5p, hsa-miR-143-3p, hsa-let-7f-5p, hsa-miR-125a-5p, hsa-miR-125b-5p, hsa-let-7i-5p, hsa-miR-23a-3p, hsa-let-7g-5p, hsa-miR-29b-3p, hsa-miR-21-5p, hsa-miR-29a-3p, hsa-miR-222-3p, hsa-miR-23b-3p hsa-miR-186-5p, hsa-miR-221-3p, hsa-miR-25-3p, hsa-miR-423-3p, hsa-miR-130a-3p, hsa-miR-199a-5p, hsa-miR-24-3p, hsa-let-7b-5p, hsa-miR-191-5p, hsa-miR-199a-3p, hsa-let-7d-5p, hsa-let-7a-3p, hsa-miR-199b-3p	1.08E-07
p53 signaling pathway	hsa-miR-130a-3p, hsa-miR-29b-3p, hsa-miR-143-3p, hsa-miR-21-5p, hsa-miR-23b-3p, hsa-miR-29a-3p, hsa-miR-221-3p, hsa-miR-34a-5p, hsa-let-7e-5p, hsa-miR-23a-3p, hsa-miR-125a-5p hsa-miR-125b-5p hsa-miR-222-3p, hsa-miR-25-3p, hsa-miR-186-5p, hsa-let-7f-5p, hsa-let-7i-5p, hsa-let-7a-5p hsa-let-7a-3p, hsa-let-7g-5p, hsa-miR-191-5p hsa-miR-199a-3p, hsa-miR-423-3p, hsa-let-7b-5p, hsa-miR-24-3p, hsa-let-7d-5p, hsa-miR-199b-3p, hsa-miR-199a-5p	1.07E-06
TGF-β signaling pathway	hsa-miR-222-3p, hsa-miR-21-5p, hsa-miR-23b-3p, hsa-miR-221-3p, hsa-let-7f-5p, hsa-miR-130a-3p, hsa-let-7i-5p, hsa-let-7e-5p, hsa-miR-23a-3p, hsa-let-7a-5p, hsa-let-7g-5p, hsa-miR-34a-5p, hsa-miR-24-3p, hsa-let-7d-5p, hsa-let-7b-5p, hsa-let-7a-3p, hsa-miR-186-5p, hsa-miR-125a-5p, hsa-miR-125b-5p, hsa-miR-25-3p, hsa-miR-199a-5p, hsa-miR-29a-3p, hsa-miR-29b-3p, hsa-miR-143-3p, hsa-miR-199a-3p, hsa-miR-199b-3p, hsa-miR-423-3p	2.05E-07
Regulation of actin cytoskeleton	hsa-miR-23b-3p, hsa-miR-21-5p, hsa-miR-29a-3p, hsa-let-7e-5p, hsa-miR-23a-3p, hsa-let-7a-5p, hsa-miR-29b-3p, hsa-miR-24-3p, hsa-miR-423-3p, hsa-let-7f-5p, hsa-miR-34a-5p, hsa-let-7i-5p, hsa-let-7g-5p, hsa-miR-25-3p, hsa-miR-130a-3p, hsa-miR-125a-5p, hsa-miR-125b-5p, hsa-let-7a-3p, hsa-miR-199a-3p hsa-miR-199b-3p, hsa-miR-221-3p, hsa-miR-186-5p, hsa-miR-199a-5p, hsa-let-7b-5p, hsa-miR-191-5p, hsa-miR-222-3p, hsa-let-7d-5p, hsa-miR-143-3p	0.0056
Wnt signaling pathway	hsa-miR-23b-3p, hsa-let-7e-5p, hsa-miR-23a-3p, hsa-miR-186-5p, hsa-let-7f-5p, hsa-miR-34a-5p, hsa-let-7i-5p, hsa-let-7a-5p, hsa-let-7g-5p, hsa-miR-191-5p, hsa-miR-24-3p, hsa-miR-25-3p, hsa-miR-130a-3p, hsa-miR-29a-3p, hsa-let-7d-5p, hsa-let-7b-5p, hsa-miR-423-3p, hsa-miR-222-3p, hsa-miR-29b-3p, hsa-miR-21-5p, hsa-miR-125a-5p, hsa-miR-125b-5p, hsa-let-7a-3p, hsa-miR-199a-3p, hsa-miR-221-3p, hsa-miR-199a-5p, hsa-miR-143-3p, hsa-miR-199b-3p	0.0110

Investigative Ophthalmology & Visual Science

Table 2. Continued

Pathway	miRNAs	P
FoxO signaling pathway	hsa-miR-25-3p, hsa-let-7f-5p, hsa-miR-199a-5p, hsa-miR-23b-3p, hsa-miR-130a-3p, hsa-miR-34a-5p, hsa-miR-23a-3p, hsa-miR-29b-3p, hsa-miR-29a-3p, hsa-miR-186-5p, hsa-miR-125a-5p, hsa-miR-125b-5p, hsa-let-7i-5p, hsa-let-7e-5p, hsa-let-7a-5p, hsa-let-7g-5p, hsa-let-7b-5p, hsa-miR-222-3p, hsa-miR-143-3p, hsa-miR-21-5p, hsa-miR-221-3p, hsa-let-7d-5p, hsa-miR-199a-3p, hsa-miR-423-3p, hsa-miR-24-3p, hsa-miR-199b-3p, hsa-let-7a-3p, hsa-miR-191-5p	0.0001
MAPK signaling pathway	hsa-miR-21-5p, hsa-miR-25-3p, hsa-let-7f-5p, hsa-let-7i-5p, hsa-let-7e-5p, hsa-miR-199a-5p, hsa-let-7a-5p, hsa-let-7a-3p, hsa-let-7g-5p, hsa-let-7d-5p, hsa-let-7b-5p, hsa-miR-24-3p, hsa-miR-143-3p, hsa-miR-23b-3p, hsa-miR-34a-5p, hsa-miR-23a-3p, hsa-miR-199a-3p, hsa-miR-29b-3p, hsa-miR-29a-3p, hsa-miR-186-5p, hsa-miR-125a-5p, hsa-miR-125b-5p, hsa-miR-130a-3p, hsa-miR-191-5p, hsa-miR-423-3p, hsa-miR-222-3p, hsa-miR-221-3p, hsa-miR-199b-3p,	0.0149
DNA replication	hsa-miR-34a-5p, hsa-miR-24-3p, hsa-miR-130a-3p, hsa-miR-125a-5p, hsa-miR-125b-5p, hsa-let-7f-5p, hsa-let-7i-5p, hsa-let-7e-5p, hsa-miR-23a-3p, hsa-let-7a-5p, hsa-let-7g-5p, hsa-miR-25-3p, hsa-miR-143-3p, hsa-miR-186-5p, hsa-miR-21-5p, hsa-miR-23b-3p, hsa-let-7b-5p, hsa-let-7d-5p, hsa-miR-222-3p, hsa-miR-199a-3p, hsa-miR-199b-3p	0.0353
Apoptosis	hsa-miR-29b-3p, hsa-miR-29a-3p, hsa-miR-222-3p, hsa-miR-221-3p, hsa-let-7f-5p, hsa-let-7i-5p, hsa-let-7a-5p, hsa-let-7g-5p, hsa-miR-191-5p, hsa-miR-130a-3p, hsa-miR-23b-3p, hsa-miR-186-5p, hsa-let-7e-5p, hsa-miR-23a-3p, hsa-let-7b-5p, hsa-miR-21-5p, hsa-miR-199a-3p, hsa-miR-125a-5p, hsa-miR-34a-5p, hsa-miR-24-3p, hsa-miR-25-3p, hsa-let-7d-5p, hsa-miR-199b-3p, hsa-miR-199a-5p, hsa-miR-125b-5p, hsa-miR-423-3p, hsa-miR-143-3p	0.0149

Table 3. Top 10 Gene Ontology (GO) Differentially Expressed miRNA Target Genes

GO ID	GO Term	Genes, *n*	P	miRNA
Biological Process				
GO:0034641	Cellular nitrogen compound metabolic process	2159	2.81075611905e-149	40
GO:0006464	Protein modification process	1086	1.44088281056e-72	39
GO:0048011	Neurotrophin Trk receptor signaling pathway	159	1.16556363144e-48	34
GO:0010467	Gene expression	284	2.84782655778e-44	36
GO:0044281	Small molecule metabolic process	976	4.39900689521e-41	40
GO:0038095	Fc epsilon receptor signaling pathway	104	5.41598305395e-38	36
GO:0007596	Blood coagulation	234	6.74538739087e-34	36
GO:0044403	Symbiosis, encompassing mutualism through parasitism	246	4.62843234897e-31	37
GO:0009056	Catabolic process	803	4.11487307476e-30	40
GO:0016032	Viral process	217	5.26143469816e-29	37
Cellular Component				
GO:0043226	Organelle	4328	3.1312118181e-266	40
GO:0005575	Cellular component	6847	6.37431086586e-43	40
GO:0043234	Protein complex	1545	3.38383127843e-30	39
GO:0005654	Nucleoplasm	525	1.2986747731e-25	39
GO:0005829	Cytosol	1095	1.95993403407e-19	39
GO:0005887	Integral component of plasma membrane	454	0.0133635354481	37
Molecular Function				
GO:0043167	Ion binding	2673	1.22613708211e-144	40
GO:0009058	Biosynthetic process	1809	1.72704360892e-102	40
GO:0001071	Nucleic acid binding transcription factor activity	528	4.28784358462e-55	38
GO:0003674	Molecular function	6801	9.56178388717e-51	40
GO:0019899	Enzyme binding	592	9.38656989729e-35	39
GO:0000988	Protein binding transcription factor activity	251	2.91055983641e-30	39
GO:0008092	Cytoskeletal protein binding	339	1.67385680699e-17	38
GO:0030234	Enzyme regulator activity	350	4.06567023231e-14	35
GO:0022857	Transmembrane transporter activity	395	1.80882242334e-05	38
GO:0030674	Protein binding, bridging	64	0.00351146153297	35

Investigative Ophthalmology & Visual Science

Acknowledgments

The authors thank Junho Kim, PhD, and Ga Eun You, MS (Research and Development Institute, Biosolution Co., Ltd.) for providing the ASC-derived exosomes.

Supported by Hallym University Medical Center Research Fund and by a grant from the National Research Foundation (NRF-2023R1A2C2002674) funded by the Korean government.

Disclosure: **Y. Ryu**, None; **J.S. Hwang**, None; **K. Bo Noh**, None; **S.H. Park**, None; **J.H. Seo**, None; **Y.J. Shin**, None

References

1. Shen L, Sun P, Zhang C, Yang L, Du L, Wu X. Therapy of corneal endothelial dysfunction with corneal endothelial cell-like cells derived from skin-derived precursors. *Sci Rep*. 2017;7:13400.
2. Faye PA, Poumeaud F, Chazelas P, et al. Focus on cell therapy to treat corneal endothelial diseases. *Exp Eye Res*. 2021;204:108462.
3. Liu X, Zheng T, Zhao C, et al. Genetic mutations and molecular mechanisms of Fuchs endothelial corneal dystrophy. *Eye Vis (Lond)*. 2021;8:24.
4. Chen C, Zhang B, Xue J, et al. Pathogenic role of endoplasmic reticulum stress in diabetic corneal endothelial dysfunction. *Invest Ophthalmol Vis Sci*. 2022;63:4.
5. Frausto RF, Swamy VS, Peh GSL, et al. Phenotypic and functional characterization of corneal endothelial cells during in vitro expansion. *Sci Rep*. 2020;10:7402.
6. Kumari R, Jat P. Mechanisms of cellular senescence: cell cycle arrest and senescence associated secretory phenotype. *Front Cell Dev Biol*. 2021;9:645593.
7. Sarugaser R, Hanoun L, Keating A, Stanford WL, Davies JE. Human mesenchymal stem cells self-renew and differentiate according to a deterministic hierarchy. *PLoS One*. 2009;4:e6498.
8. Zhou Y, Yamamoto Y, Xiao Z, Ochiya T. The immunomodulatory functions of mesenchymal stromal/stem cells mediated via paracrine activity. *J Clin Med*. 2019;8:1025.
9. Yao Y, Huang J, Geng Y, et al. Paracrine action of mesenchymal stem cells revealed by single cell gene profiling in infarcted murine hearts. *PLoS One*. 2015;10:e0129164.
10. Sarhadi VK, Daddali R, Seppanen-Kaijansinkko R. Mesenchymal stem cells and extracellular vesicles in osteosarcoma pathogenesis and therapy. *Int J Mol Sci*. 2021;22:11035.
11. Yu B, Zhang X, Li X. Exosomes derived from mesenchymal stem cells. *Int J Mol Sci*. 2014;15:4142–4157.
12. Gonzalez-Cubero E, Gonzalez-Fernandez ML, Olivera ER, Villar-Suarez V. Extracellular vesicle and soluble fractions of adipose tissue-derived mesenchymal stem cells secretome induce inflammatory cytokines modulation in an in vitro model of discogenic pain. *Spine J*. 2022;22:1222–1234.
13. Trzyna A, Banás-Zabczyk A. Adipose-derived stem cells secretome and its potential application in "stem cell-free therapy". *Biomolecules*. 2021;11:878.
14. Jiao Z, Ma Y, Zhang Q, et al. The adipose-derived mesenchymal stem cell secretome promotes hepatic regeneration in miniature pigs after liver ischaemia-reperfusion combined with partial resection. *Stem Cell Res Ther*. 2021;12:218.
15. Shin YJ, Cho DY, Chung TY, Han SB, Hyon JY, Wee WR. Rapamycin reduces reactive oxygen species in cultured human corneal endothelial cells. *Curr Eye Res*. 2011;36:1116–1122.
16. Merlini L, Angelin A, Tiepolo T, et al. Cyclosporin A corrects mitochondrial dysfunction and muscle apoptosis in patients with collagen VI myopathies. *Proc Natl Acad Sci USA*. 2008;105:5225–5229.
17. Hwang JS, Ma DJ, Choi J, Shin YJ. COL8A2 regulates the fate of corneal endothelial cells. *Invest Ophthalmol Vis Sci*. 2020;61:26.
18. Kim J, You GE, Woo M, Chang NH, Lee J. Discovery of lactoferrin as a stimulant for hADSC-derived EV secretion and proof of enhancement of resulting EVs through skin model. *Int J Mol Sci*. 2021;22:10993.
19. Hsu SY, Wen ZH, Shih PC, et al. Sinularin induces oxidative stress-mediated apoptosis and mitochondrial dysfunction, and inhibits angiogenesis in glioblastoma cells. *Antioxidants (Basel)*. 2022;11:1433.
20. Zhang Y, Ouyang J, Zhan L, et al. Autophagy in homocysteine-induced HUVEC senescence. *Exp Ther Med*. 2023;26:354.
21. Han SB, Ang H, Balehosur D, et al. A mouse model of corneal endothelial decompensation using cryoinjury. *Mol Vis*. 2013;19:1222–1230.
22. Schmidt JA, Rinaldi S, Ferrari P, et al. Metabolic profiles of male meat eaters, fish eaters, vegetarians, and vegans from the EPIC-Oxford cohort. *Am J Clin Nutr*. 2015;102:1518–1526.
23. Park S, Leonard BC, Raghunathan VK, et al. Animal models of corneal endothelial dysfunction to facilitate development of novel therapies. *Ann Transl Med*. 2021;9:1271.
24. Georgakilas G, Vlachos IS, Zagganas K, et al. DIANA-miRGen v3.0: accurate characterization of microRNA promoters and their regulators. *Nucleic Acids Res*. 2016;44:D190–D195.
25. Kanehisa M, Furumichi M, Sato Y, Ishiguro-Watanabe M, Tanabe M. KEGG: integrating viruses and cellular organisms. *Nucleic Acids Res*. 2021;49:D545–D551.
26. Kanehisa M, Goto S. KEGG: kyoto encyclopedia of genes and genomes. *Nucleic Acids Res*. 2000;28:27–30.
27. Li Z, Liu T, Ma J, et al. TGF-β induces corneal endothelial senescence via increase of mitochondrial reactive oxygen species in chronic corneal allograft failure. *Aging (Albany NY)*. 2018;10:3474–3485.
28. Yu AL, Fuchshofer R, Kook D, Kampik A, Bloemendal H, Welge-Lussen U. Subtoxic oxidative stress induces senescence in retinal pigment epithelial cells via TGF-β release. *Invest Ophthalmol Vis Sci*. 2009;50:926–935.
29. Wu CC, Tzeng CY, Chang CY, et al. NMDA receptor inhibitor MK801 alleviated pro-inflammatory polarization of BV-2 microglia cells. *Eur J Pharmacol*. 2023;955:175927.
30. Loh CY, Chai JY, Tang TF, et al. The E-cadherin and N-cadherin switch in epithelial-to-mesenchymal transition: signaling, therapeutic implications, and challenges. *Cells*. 2019;8:1118.
31. Cheng D, Jin L, Chen Y, Xi X, Guo Y. YAP promotes epithelial mesenchymal transition by upregulating Slug expression in human colorectal cancer cells. *Int J Clin Exp Pathol*. 2020;13:701–710.
32. Akrida I, Bravou V, Papadaki H. The deadly cross-talk between Hippo pathway and epithelial-mesenchymal transition (EMT) in cancer. *Mol Biol Rep*. 2022;49:10065–10076.
33. Runwal G, Stamatakou E, Siddiqi FH, Puri C, Zhu Y, Rubinsztein DC. LC3-positive structures are prominent in autophagy-deficient cells. *Sci Rep*. 2019;9:10147.
34. Sun X, Kaufman PD. Ki-67: more than a proliferation marker. *Chromosoma*. 2018;127:175–186.
35. Bernal A, Arranz L. Nestin-expressing progenitor cells: function, identity and therapeutic implications. *Cell Mol Life Sci*. 2018;75:2177–2195.

Investigative Ophthalmology & Visual Science

36. Janockova J, Slovinska L, Harvanova D, Spakova T, Rosocha J. New therapeutic approaches of mesenchymal stem cells-derived exosomes. *J Biomed Sci*. 2021;28:39.
37. Rajool Dezfuly A, Safaee A, Salehi H. Therapeutic effects of mesenchymal stem cells-derived extracellular vesicles' miRNAs on retinal regeneration: a review. *Stem Cell Res Ther*. 2021;12:530.
38. Tsuji W, Rubin JP, Marra KG. Adipose-derived stem cells: implications in tissue regeneration. *World J Stem Cells*. 2014;6:312–321.
39. Vizoso FJ, Eiro N, Cid S, Schneider J, Perez-Fernandez R. Mesenchymal stem cell secretome: toward cell-free therapeutic strategies in regenerative medicine. *Int J Mol Sci*. 2017;18:1852.
40. Zhao S, Fei X, Liu T, Liu Y. Low temperature induces cryoinjury in mouse corneal endothelial cells by stimulating the Stk11-p53 signal pathway. *Mol Med Rep*. 2015;12:6612–6616.
41. Akhbanbetova A, Nakano S, Littlechild SL, et al. A surgical cryoprobe for targeted transcorneal freezing and endothelial cell removal. *J Ophthalmol*. 2017;2017:5614089.
42. Xiong M, Zhang Q, Hu W, et al. Exosomes from adipose-derived stem cells: the emerging roles and applications in tissue regeneration of plastic and cosmetic surgery. *Front Cell Dev Biol*. 2020;8:574223.
43. Samanta S, Rajasingh S, Drosos N, Zhou Z, Dawn B, Rajasingh J. Exosomes: new molecular targets of diseases. *Acta Pharmacol Sin*. 2018;39:501–513.
44. Ferguson SW, Wang J, Lee CJ, et al. The microRNA regulatory landscape of MSC-derived exosomes: a systems view. *Sci Rep*. 2018;8:1419.
45. Day AJ, Milner CM. TSG-6: a multifunctional protein with anti-inflammatory and tissue-protective properties. *Matrix Biol*. 2019;78-79:60–83.
46. Tseng HW, Samuel SG, Schroder K, Levesque JP, Alexander KA. Inflammasomes and the IL-1 family in bone homeostasis and disease. *Curr Osteoporos Rep*. 2022;20:170–185.
47. Saraiva M, O'Garra A. The regulation of IL-10 production by immune cells. *Nat Rev Immunol*. 2010;10:170–181.
48. Cecerska-Heryc E, Goszka M, Serwin N, et al. Applications of the regenerative capacity of platelets in modern medicine. *Cytokine Growth Factor Rev*. 2022;64:84–94.
49. Thuan DTB, Zayed H, Eid AH, et al. A potential link between oxidative stress and endothelial-to-mesenchymal transition in systemic sclerosis. *Front Immunol*. 2018;9:1985.
50. Xu X, Zheng L, Yuan Q, et al. Transforming growth factor-β in stem cells and tissue homeostasis. *Bone Res*. 2018;6:2.
51. Chen X, Zhang X, Jiang Y, et al. YAP1 activation promotes epithelial-mesenchymal transition and cell survival of renal cell carcinoma cells under shear stress. *Carcinogenesis*. 2022;43:301–310.
52. Wang M, Dai M, Wang D, Xiong W, Zeng Z, Guo C. The regulatory networks of the Hippo signaling pathway in cancer development. *J Cancer*. 2021;12:6216–6230.
53. Tofino-Vian M, Guillen MI, Perez Del Caz MD, Castejon MA, Alcaraz MJ. Extracellular vesicles from adipose-derived mesenchymal stem cells downregulate senescence features in osteoarthritic osteoblasts. *Oxid Med Cell Longev*. 2017;2017:7197598.
54. Liao CM, Luo T, von der Ohe J, de Juan Mora B, Schmitt R, Hass R. Human MSC-derived exosomes reduce cellular senescence in renal epithelial cells. *Int J Mol Sci*. 2021;22:13562.
55. Yan W, Diao S, Fan Z. The role and mechanism of mitochondrial functions and energy metabolism in the function regulation of the mesenchymal stem cells. *Stem Cell Res Ther*. 2021;12:140.
56. Ji Y, Di W, Yang Q, Lu Z, Cai W, Wu J. Inhibition of autophagy increases proliferation inhibition and apoptosis induced by the PI3K/mTOR inhibitor NVP-BEZ235 in breast cancer cells. *Clin Lab*. 2015;61:1043–1051.
57. Guerra F, Guaragnella N, Arbini AA, Bucci C, Giannattasio S, Moro L. Mitochondrial dysfunction: a novel potential driver of epithelial-to-mesenchymal transition in cancer. *Front Oncol*. 2017;7:295.
58. Guha M, Srinivasan S, Ruthel G, et al. Mitochondrial retrograde signaling induces epithelial-mesenchymal transition and generates breast cancer stem cells. *Oncogene*. 2014;33:5238–5250.
59. Liang C, Xu J, Meng Q, et al. TGFB1-induced autophagy affects the pattern of pancreatic cancer progression in distinct ways depending on SMAD4 status. *Autophagy*. 2020;16:486–500.
60. Lazova R, Camp RL, Klump V, Siddiqui SF, Amaravadi RK, Pawelek JM. Punctate LC3B expression is a common feature of solid tumors and associated with proliferation, metastasis, and poor outcome. *Clin Cancer Res*. 2012;18:370–379.
61. D'Arcy MS. Cell death: a review of the major forms of apoptosis, necrosis and autophagy. *Cell Biol Int*. 2019;43:582–592.
62. Buono L, Scalabrin S, De Iuliis M, et al. Mesenchymal stem cell-derived extracellular vesicles protect human corneal endothelial cells from endoplasmic reticulum stress-mediated apoptosis. *Int J Mol Sci*. 2021;22:4930.
63. Nguyen DD, Lai JY. Synthesis, bioactive properties, and biomedical applications of intrinsically therapeutic nanoparticles for disease treatment. *Chem Eng J*. 2022;435:134970.
64. Zhou J, Wang X, Wang M, et al. The lysine catabolite saccharopine impairs development by disrupting mitochondrial homeostasis. *J Cell Biol*. 2019;218:580–597.
65. Anderson KA, Hirschey MD. Mitochondrial protein acetylation regulates metabolism. *Essays Biochem*. 2012;52:23–35.
66. Li Z, Wang Y, Xiang S, et al. Chondrocytes-derived exosomal miR-8485 regulated the Wnt/β-catenin pathways to promote chondrogenic differentiation of BMSCs. *Biochem Biophys Res Commun*. 2020;523:506–513.
67. Li W, Han Y, Zhao Z, et al. Oral mucosal mesenchymal stem cell-derived exosomes: a potential therapeutic target in oral premalignant lesions. *Int J Oncol*. 2019;54:1567–1578.
68. Ouyang C, Huang L, Ye X, Ren M, Han Z. Overexpression of miR-1298 attenuates myocardial ischemia-reperfusion injury by targeting PP2A. *J Thromb Thrombolysis*. 2022;53:136–148.
69. Ruibin W, Zheng X, Chen J, Zhang X, Yang X, Lin Y. Micro RNA-1298 opposes the effects of chronic oxidative stress on human trabecular meshwork cells via targeting on EIF4E3. *Biomed Pharmacother*. 2018;100:349–357.
70. Mu M, Niu W, Zhang X, Hu S, Niu C. LncRNA BCYRN1 inhibits glioma tumorigenesis by competitively binding with miR-619-5p to regulate CUEDC2 expression and the PTEN/AKT/p21 pathway. *Oncogene*. 2020;39:6879–6892.
71. Jiang M, Sun Z, Dang E, et al. TGFβ/SMAD/microRNA-486-3p signaling axis mediates keratin 17 expression and keratinocyte hyperproliferation in psoriasis. *J Invest Dermatol*. 2017;137:2177–2186.
72. Zhou H, Wang K, Hu Z, Wen J. TGF-β1 alters microRNA profile in human gastric cancer cells. *Chin J Cancer Res*. 2013;25:102–111.
73. Han YL, Yin JJ, Cong JJ. Downregulation of microRNA-193-3p inhibits the progression of intrahepatic cholangiocarcinoma cells by upregulating TGFBR3. *Exp Ther Med*. 2018;15:4508–4514.

Investigative Ophthalmology & Visual Science

74. Yan B, Zhao JL. miR-1228 prevents cellular apoptosis through targeting of MOAP1 protein. *Apoptosis*. 2012;17:717–724.
75. Jia L, Wu J, Zhang L, et al. Restoration of miR-1228* expression suppresses epithelial-mesenchymal transition in gastric cancer. *PLoS One*. 2013;8:e58637.
76. Yan K, An T, Zhai M, et al. Mitochondrial miR-762 regulates apoptosis and myocardial infarction by impairing ND2. *Cell Death Dis*. 2019;10:500.
77. Qiang J, Tao F, Bao W, et al. miR-489-3p regulates the oxidative stress response in the liver and gill tissues of hybrid yellow catfish (*Pelteobagrus fulvidraco*♀ × *P. vachelli*♂) under Cu^{2+} exposure by targeting *Cu/Zn-SOD*. *Front Physiol*. 2019;10:868.
78. Ye Y, Wang P, Zhou F. miR-489-3p inhibits TLR4/NF-κB signaling to prevent inflammation in psoriasis. *Exp Ther Med*. 2021;22:744.
79. Li J, Dong S, Ye M, et al. MicroRNA-489-3p represses hepatic stellate cells activation by negatively regulating the JAG1/Notch3 signaling pathway. *Dig Dis Sci*. 2021;66:143–150.
80. Pan Y, Shu X, Sun L, et al. miR196a5p modulates gastric cancer stem cell characteristics by targeting Smad4. *Int J Oncol*. 2017;50:1965–1976.
81. Sutliff AK, Watson CJW, Chen G, Lazarus P. Regulation of UGT2A1 by miR-196a-5p and miR-196b-5p. *J Pharmacol Exp Ther*. 2019;369:234–243.
82. Liu P, Wang C, Ma C, Wu Q, Zhang W, Lao G. MicroRNA-23a regulates epithelial-to-mesenchymal transition in endometrial endometrioid adenocarcinoma by targeting SMAD3. *Cancer Cell Int*. 2016;16:67.
83. Yang L, Du X, Liu L, Cao Q, Pan Z, Li Q. miR-1306 mediates the feedback regulation of the TGF-β/SMAD signaling pathway in granulosa cells. *Cells*. 2019;8:298.
84. Li Y, He J, Yu L, et al. Hsa-miR-1290 is associated with stemness and invasiveness in prostate cancer cell lines by targeting RORA. *Andrologia*. 2022;54:e14396.
85. Markopoulos GS, Roupakia E, Tokamani M, et al. Senescence-associated microRNAs target cell cycle regulatory genes in normal human lung fibroblasts. *Exp Gerontol*. 2017;96:110–122.
86. Taguchi YH. Inference of target gene regulation via miRNAs during cell senescence by using the MiRaGE server. *Aging Dis*. 2012;3:301–306.
87. Suh N. MicroRNA controls of cellular senescence. *BMB Rep*. 2018;51:493–499.
88. Ma J, Huang W, Zhu C, et al. miR-423-3p activates FAK signaling pathway to drive EMT process and tumor growth in lung adenocarcinoma through targeting CYBRD1. *J Clin Lab Anal*. 2021;35:e24044.
89. Liang YK, Lin HY, Dou XW, et al. MiR-221/222 promote epithelial-mesenchymal transition by targeting Notch3 in breast cancer cell lines. *NPJ Breast Cancer*. 2018;4:20.
90. Wang D, Sang Y, Sun T, et al. Emerging roles and mechanisms of microRNA2223p in human cancer (Review). *Int J Oncol*. 2021;58:20.
91. Varga ZV, Kupai K, Szucs G, et al. MicroRNA-25-dependent up-regulation of NADPH oxidase 4 (NOX4) mediates hypercholesterolemia-induced oxidative/nitrative stress and subsequent dysfunction in the heart. *J Mol Cell Cardiol*. 2013;62:111–121.
92. Hu Z, Klein JD, Mitch WE, Zhang L, Martinez I, Wang XH. MicroRNA-29 induces cellular senescence in aging muscle through multiple signaling pathways. *Aging (Albany NY)*. 2014;6:160–175.
93. Wang J, Zhu M, Ye L, Chen C, She J, Song Y. MiR-29b-3p promotes particulate matter-induced inflammatory responses by regulating the C1QTNF6/AMPK pathway. *Aging (Albany NY)*. 2020;12:1141–1158.
94. Muller-Deile J, Gellrich F, Schenk H, et al. Overexpression of TGF-β inducible microRNA-143 in zebrafish leads to impairment of the glomerular filtration barrier by targeting proteoglycans. *Cell Physiol Biochem*. 2016;40:819–830.
95. Zhu X, Liu D, Li G, et al. Exosomal miR-140-3p and miR-143-3p from TGF-β1-treated pancreatic stellate cells target BCL2 mRNA to increase β-cell apoptosis. *Mol Cell Endocrinol*. 2022;551:111653.
96. Zhang Y, Huang S, Yang G, Zou L, Huang X, Liu S. The role of miRNAs during endoplasmic reticulum stress induced apoptosis in digestive cancer. *J Cancer*. 2021;12:6787–6795.
97. Tian X, Fei Q, Du M, et al. miR-130a-3p regulated TGF-β1-induced epithelial-mesenchymal transition depends on SMAD4 in EC-1 cells. *Cancer Med*. 2019;8:1197–1208.
98. Liu Y, Ding Y, Hou Y, Yu T, Nie H, Cui Y. The miR-130a-3p/TGF-βRII axis participates in inhibiting the differentiation of fibroblasts induced by TGF-β1. *Front Pharmacol*. 2021;12:732540.
99. Dai X, Fang M, Li S, Yan Y, Zhong Y, Du B. miR-21 is involved in transforming growth factor β1-induced chemoresistance and invasion by targeting PTEN in breast cancer. *Oncol Lett*. 2017;14:6929–6936.
100. An Y, Zhang Q, Li X, Wang Z, Li Y, Tang X. Upregulated microRNA miR-21 promotes the progression of lung adenocarcinoma through inhibition of KIBRA and the Hippo signaling pathway. *Biomed Pharmacother*. 2018;108:1845–1855.
101. Barbollat-Boutrand L, Joly-Tonetti N, Dos Santos M, et al. MicroRNA-23b-3p regulates human keratinocyte differentiation through repression of TGIF1 and activation of the TGF-β-SMAD2 signalling pathway. *Exp Dermatol*. 2017;26:51–57.
102. Zhou W, Xu J, Wang C, Shi D, Yan Q. miR-23b-3p regulates apoptosis and autophagy via suppressing SIRT1 in lens epithelial cells. *J Cell Biochem*. 2019;120:19635–19646.
103. Xia J, Li S, Ma D, Guo W, Long H, Yin W. MicroRNA293p regulates the β-catenin pathway by targeting IGF1 to inhibit the proliferation of prolactinoma cells. *Mol Med Rep*. 2021;23:432.
104. Hong H, Tao T, Chen S, et al. MicroRNA-143 promotes cardiac ischemia-mediated mitochondrial impairment by the inhibition of protein kinase Cepsilon. *Basic Res Cardiol*. 2017;112:60.
105. Wei WF, Zhou CF, Wu XG, et al. MicroRNA-221-3p, a TWIST2 target, promotes cervical cancer metastasis by directly targeting THBS2. *Cell Death Dis*. 2017;8:3220.
106. He W, Feng J, Zhang Y, Wang Y, Zang W, Zhao G. microRNA-186 inhibits cell proliferation and induces apoptosis in human esophageal squamous cell carcinoma by targeting SKP2. *Lab Invest*. 2016;96:317–324.
107. Liang J, Zhang Y, Jiang G, et al. MiR-138 induces renal carcinoma cell senescence by targeting EZH2 and is downregulated in human clear cell renal cell carcinoma. *Oncol Res*. 2013;21:83–91.
108. Manakanatas C, Ghadge SK, Agic A, et al. Endothelial and systemic upregulation of miR-34a-5p fine-tunes senescence in progeria. *Aging (Albany NY)*. 2022;14:195–224.
109. He S, Huang Y, Dong S, et al. MiR-199a-3p/5p participated in TGF-β and EGF induced EMT by targeting DUSP5/MAP3K11 in pterygium. *J Transl Med*. 2020;18:332.
110. Nagpal N, Ahmad HM, Chameettachal S, Sundar D, Ghosh S, Kulshreshtha R. HIF-inducible miR-191 promotes migration in breast cancer through complex regulation of TGFβ-signaling in hypoxic microenvironment. *Sci Rep*. 2015;5:9650.

Investigative Ophthalmology & Visual Science

111. Yu S, Lu Y, Zong M, Tan Q, Fan L. Hypoxia-induced miR-191-C/EBPβ signaling regulates cell proliferation and apoptosis of fibroblast-like synoviocytes from patients with rheumatoid arthritis. *Arthritis Res Ther*. 2019;21:78.
112. Wei L, He Y, Bi S, Li X, Zhang J, Zhang S. miRNA-199b-3p suppresses growth and progression of ovarian cancer via the CHK1/E-cadherin/EMT signaling pathway by targeting ZEB1. *Oncol Rep*. 2021;45:569–581.
113. Zhang R, Wang M, Sui P, Ding L, Yang Q. Upregulation of microRNA-574-3p in a human gastric cancer cell line AGS by TGF-β1. *Gene*. 2017;605:63–69.
114. Vittoria MA, Shenk EM, O'Rourke KP, et al. A genome-wide microRNA screen identifies regulators of tetraploid cell proliferation. *Mol Biol Cell*. 2018;29:1682–1692.

Investigative Ophthalmology & Visual Science